電子
385

Epitaxial Growth of Gallium Antimonide Self-assembled Quantum Dots and their Optical Properties

(ガリウムアンチモン自己組織化量子ドットの形成とその光物性)

A Dissertation Submitted in Partial Fulfillment
of the Requirements for the Degree of

Doctor of Engineering
in
Electronic Engineering

UNIVERSITY of TOKYO

by

Kenji SUZUKI

December 18, 1998

Dissertation Supervisor
Professor Yasuhiko ARAKAWA

To my parents

Preface

This thesis presents a part of the research carried out at the Institute of Industrial Science (IIS) and the Research Center for Advanced Science and Technology (RCAST) of the University of Tokyo. Professor Yasuhiko ARAKAWA has supervised this research while the author was a student of the graduate school in Department of Electronic Engineering of the University of Tokyo from April 1996 through March 1999.

In this thesis, a study on GaSb self-assembled quantum dots grown by molecular beam epitaxy and their optical properties was described.

Tokyo, Japan
December 18, 1998

Kenji SUZUKI

Typeset using LaTeX

Acknowledgments

The author would like to thank not only those who have assisted his research in this dissertation but also his parents and all his friends for their encouragement.

Professor Yasuhiko ARAKAWA, the dissertation supervisor, of the Research Center for Advanced Science and Technology (RCAST) in the University of Tokyo, has provided the author with plenty of support and encouragement from April 1996 through March 1999. His knowledge and insights have propelled the author's learning. Besides, generosities and enthusiasm have touched the author's heart.

It is also his great pleasure to acknowledge Professor T. NISHINAGA, Professor H. SAKAKI, Professor K. HIRAKAWA, Professor T. KAMIYA, Professor Y. NAKANO, Professor T. TAKAHASHI, and Professor T. SOMEYA, the committee of this thesis, for stimulating discussion and their encouragement.

On November 1997, the author visited the Hughes Research Laboratory, in order to learn a GaSb growth by molecular beam epitaxy and semiconductor lasers for long wave length. The author acknowledge Dr. D. H. CHOW, Dr. R. H. MILES, and Professor J. N. SCHULMAN for their teaching and their encouragement.

On April 1998, the author visited the University of California Santa Barbara. The author acknowledge Professor J. E. BOWERS, Ms. M. S. MINSKY, and Dr.S. B. FLEISHER for the collaboration of time-resolved photoluminescence measurements.

The author was in the Chiba University during the undergraduate and the master course. The author wishes to thank Professor H. OKAMOTO, Professor T. MATSUSUE, Professor S. S. SHIRATORI and Professor K. OHTAKA for the education of experimental and theoretical physics.

The author would like to thank Dr. R. A. HOGG for the enjoyable collaboration and plentiful efforts. This research has been carried out with the help of his supports and fruitful discussion. The author wishes to thank Dr. Y. Toda for his collaboration in magneto-photoluminescence measurements, Mr. K. TACHIBANA for his collaboration in molecular beam epitaxy, Mr. S. KAKO for his collaboration in time-resolved photoluminescence measurements, Mr. L. FINGER for his collaboration in photoluminescence excitation measurements, Dr. T. SAITO, Dr. X. LI, and Dr. M. OZAKI for their help with the theoretical calculations, and the staff of the calculation centre in the IIS for the kind assistance on Unix system.

The author will always remember their supports from colleagues :
Mr. M. NISHIOKA, Mr. S. ISHIDA, Dr. Y. KONDOH, Dr. Y. NAGAMUNE, Dr. T. NODA, Dr Y. OHNO, Dr. M. NARIHIRO,Dr. J. HARRIS, Monsieur J. PODLECKI, Monsieur S. KRAWCZYK, Dr. T. NODA, Professor B. SHEN, Dr. X. P.FENG, Dr. F. SOGAWA, Dr. T. ARAKAWA, Professor Z. L. ZHANG, Mr. H. WATABE, Mr. N. SEKINE, Mr. G. YUSA, Mr. D. KISHIMOTO, Mr. R. SCHUR, Mr. M. NIELSEN, Mr. H. HAYASHI, Mr.Y. KATOH, Mr.S. SHINOMORI, Mr.Y. MATSUDA, Mr.K. YAMANAKA, Mr.O. MORIWAKI, Mr.J. TATEBAYASHI, Ms.K. ARAI, Ms. N. KAYA, and Ms. S. YAMASAKI.

Je n'oublierai pas de remercier Mademoiselle H.BRISSET et Monsieur S.KHALFALLAH pour m'avoir enseigner le français.

This work was supported in part by the Research for the Future Program of the Japan Society for the Promotion of Science (Project No.JSPS-RFTF96P00201), Grant in-aid for Scientific Research (A) by Ministry of Education, Science and Culture, and University-Industry Joint Project on Quantum Nanoelectronics.

Finally, this research could not be possible without their kind encouragement of my parents and Miss Haruka KUDOH.

"Epitaxial Growth of Gallium Antimonide
Self-assembled Quantum Dots and their Optical Properties"

Table of Contents

Dedication i

Preface ii

Acknowledgments iii

I. Introduction

1.1 Research on Quantum Dots 1

1.2 Band Alignment in Real Space 5

1.3 Device Applications of GaSb 9

1.4 Objectives and Scope of Present Works 11

1.5 Synopses of Chapters 12

Bibliography 15

II. Epitaxial Growth of Self-assembled GaSb/GaAs Quantum Dots

2.1 Introduction 18

2.2 Epitaxial Growth Conditions 19

2.3 Discussion on the Epitaxial Growth Conditions 22

2.4 Density Control of Quantum Dots 25

2.5 Stacked Structures 29

2.6 Summary 33

Bibliography 34

III. Photoluminescence of Type-II GaSb/GaAs Quantum Dots

3.1 Introduction 36

3.2 Photoluminescence 37

3.3 Excitation Intensity Dependence 41

3.4 Excitation Energy Dependence 42

3.5 Temperature Dependence 47

3.6 Photoluminescence Excitation Spectrum 50

3.7 Type-II Staggered Band Alignment 52

3.8 Summary 55

Bibliography 57

IV. Time-resolved Photoluminescence of Type-II GaSb/GaAs Quantum Dots

4.1 Introduction 60

4.2 Time-resolved Photoluminescence Setup 61

4.3 Time-resolved Photoluminescence 64

4.4 Excitation Intensity Dependence 67

4.5 Conduction Band Offset 68

4.6 Summary 71

Bibliography 72

V. Magneto-photoluminescence of Type-II GaSb/GaAs Quantum Dots

5.1 Introduction 73

5.2 Photoluminescence in Magnetic Fields 74

5.3 Diamagnetic Shifts 76

5.4 Oscillator Strength 79

5.5 Exciton Binding Energy 80

5.6 Summary 81

Bibliography 82

VI. Type-I InAs and Type-II GaSb Coupled Quantum Dots

6.1 Introduction 84

6.2 Epitaxial Growth of Coupled Quantum Dots 85

6.3 Photoluminescence of InAs and GaSb Coupled Quantum Dots 85

6.4 Summary 88

Bibliography 89

VII. InSb/GaSb Self-assembled Dots

7.1 Introduction 90

7.2 Epitaxial Growth of GaSb Buffer Layers on GaAs with a Superlattice 92

7.3 Surface Morphology of GaSb Buffer Layers on GaAs with a Superlattice 93

7.4 The Strain in a GaSb/GaAs Superlattice 95

7.5 Epitaxial Growth of InSb/GaSb Dots 96

7.6 Summary 98

Bibliography 99

VIII. Conclusions

8.1 Summary 100

8.2 Future Prospect 102

Appendix

A. Photoluminescence of Nonequilibrium Carriers in Type-II Band Alignment 103

B. Material Parameters of GaSb 105

Publications

1. Journals 109

2. International Conferences 111

3. Domestic Conferences 113

Chapter 1

Introduction

1.1 Research on Quantum Dots

In 1969, research on quantum structures started with a proposal of semiconductor superlattice by L. Esaki and R. Tsu [1, 2]. Semiconductor heterostructures are of considerable technological importance for their novel electronic and optical devices. It has the great flexibility in design that allows by variation of alloying concentration, the thickness of the layers, and the state of strain. Activities in this frontier of semiconductor physics give immeasurable stimulus to device physics, leading to transport and optoelectronic devices.

In 1982, Y. Arakawa and H. Sakaki proposed a concept of quantum box lasers [3]. Since then, zero-dimensional semiconductor structures have received a great attention. Semiconductor quantum dots are expected to exhibit exciting new electronic and optical properties such as an atomic like δ-function density of state (DOS). The optical properties of the quantum dots are expected to exhibit large oscillator strengths and consequently high photon emission difference due to their δ-like DOS. This is attractive for optoelectronic devices such as lasers which should have a higher differential gain, lower threshold current density, and a higher temperature stability than conventional quantum well lasers. [3, 4]

In 1994, quantum dot lasers were realized by several groups in which self-assembled qunatum dots were exploited. [5, 6, 7] Self-assembled quantum dots allowed it. The details will be mentioned in the next paragraph. However, to make high efficiency lasers, it is still necessary to make uniformly size dots, increase dot densities, and improve spontaneous emission efficiency.

Year	Progress
1969	Proposal of semiconductor superlattice by L.Esaki and R.Tu. [1, 2]
1982	Proposal of quantum dot lasers by Y.Arakawa and H.Sakaki. [3]
1994	Quantum dot lasers were realized. [5, 6, 7]

Table 1.1 : History of research on quantum dots.

Self-assembled Quantum Dots Structures

Epitaxial growth techniques, such as molecular beam epitaxy (MBE) and metalorganic vapor phase epitaxy (MOVPE), have become so sophisticated that extremely high quality interfaces can be produced even for material system with lattice mismatches of several percent. In order to realize low dimensional semiconductor structures, various approaches have been reported.

Recently, it has been reported that it is possible to directly grow quantum dots in highly strained semiconductors. [8, 9] In Table 1-1, various self-assembled quantum dots are shown. For example, InAs self-assembled quantum dots on GaAs, were grown by Stranski-Krastanow growth[10], which produces defect free quantum dots

with mean diameter reaching ~20 nm [9].

Heteroepitaxy is usually categorized by the following three growth modes :

(1) Frank-van der Merwe growth in which the crystal grows layer by layer (2D),

(2) Volmer-Weber growth in which islands form on thesurface (3D), and

(3) Stranski-Krastanow growth which starts as a layer by layer growth, then after a few monolayers, islands are formed. (2D to 3D).

Epitaxial growth depends on the inter facial energy and degree of lattice mismatch. Between materials with same lattice constant, the heteroepitaxy is in Frank-van der Merwe growth mode. It is used for producing two-dimensional layered structures, such as a conventional AlGaAs/GaAs quantum wells. Semiconductors lattice constants can be grown pseudomorphically without dislocations at the interface, if the growth layer is thinner than a certain critical thickness. However, between large lattice constant materials, Stranski-Krastanow growth mode or Frank-van der Merwe growth mode occur.

Recently, this Stranski-Krastanow growth mode realizes quantum dots with the order of 10 nm scale, so that quantum size effects could be expected. Dots are epitaxially formed on highly mismatched substrate. It was found to grow under the Stranski-Krastanow mode. A layer was first grown in 2D, and 3D islands were formed after some critical thickness was reached. These dots were introduced to accommodate the strain energy without creating dislocations between the 3D dots and the 2D wetting layer. These dots are epitaxially and coherently grown. The term "self-assembled" is used to refer to these kinds of dots. It is also possible to grow zero-dimensional structures without any patterning at all. However,epitaxial growth of self-assembled quantum dots are still immature. It is required to improve

the size uniformity and increase the density for quantum dot lasers and to realize *band structure engineering.*

Materials	Strain (%)	Reference	Year
InAs/GaAs	~7	L.Goldstein *et al.*, [11]	1985
InGaAs/GaAs	~4	Oshinowo *et al.*, Univ. of Tokyo[12]	1994
ZnSe/ZnS		M.C.Harris *et al.*[13]	1997
CdS/ZnSe	~3	M.Kobayashi *et al.*[14]	1998
Si/Ge	~4	P.Schittenhelm *et al.*[15]	1995
Si/SiC	~20	Fissel *et al.*[16]	1997
InP/GaAs		M.Sopanen*et al.*, Helsinki Univ.[17]	1997
GaN/Si/AlGaN	~0.2	Xu-Q. Shen *et al.*, RIKEN [18]	1998
InSb/InP	~10	Utzmeieret *et al.*, Spain[19]	1996
AlSb/GaAs	~8	Bennett *et al.*, Naval Resarch Lab.[20]	1996
InSb/GaAs	~15	Bennett *et al.*, Naval Resarch Lab.[20]	1996
InSb/GaSb	~6	M. Yano *et al.*, Osaka Inst. Univ.[21]	1998
GaSb/GaAs	~8	Bennett *et al.*, Naval Resarch Lab.[20]	1996

Table 1.2 : Various self-assembled quantum dots.

1.2 Band Alignment in Real Space

In this section, band structures in semiconductors related to GaSb are exhibited. There are three important points, although lots of physical phenomena can modify

the electronic band structure. These are used for *band structure engineering.* Three phenomena involve using of:

(1) alloying of two or more semiconductor,

(2) heterostructures to cause quantum confinement, and

(3) built-in strain via lattice mismatched epitaxy.

These three concepts are used for improving performance in electronic and optical devices.

Figure 1.1 shows the bandgap at 300 K as a function of the lattice constant for some semiconductors of GaSb and related materials. The lines represent alloys with solid and dashed lines denoting direct and indirect gap semiconductors, respectively. The lattice constants in compounds of antimony are larger than that of GaAs. An InSb has a the largest lattice constant and 6.88 μm (0.18 eV) emission. The lattice constants of an AlSb and an InAs are close to a GaSb substrate. It allows high quality epitaxial layer. In k-space, almost compounds of antimony except an AlSb and the alloying has direct transition at the Γ point. The AlSb and the alloying have indirect transition at the X point. In particular, it is very useful for lasers in long wavelength (a few μm region) and for high-mobility transistor. It is most due to small band gap and light effective masses [See Appendix B from [22]].

Since 1977, the InAs/GaSb system [23, 24, 25] was investigated because of its extraordinary band edge relationship at the interface, called type-II misaligned band alignment. The evidence was confirmed by far-infrared magneto-absorption experiments [26]. In GaSb/InAs quantum wells, the unique band edge relationship allows

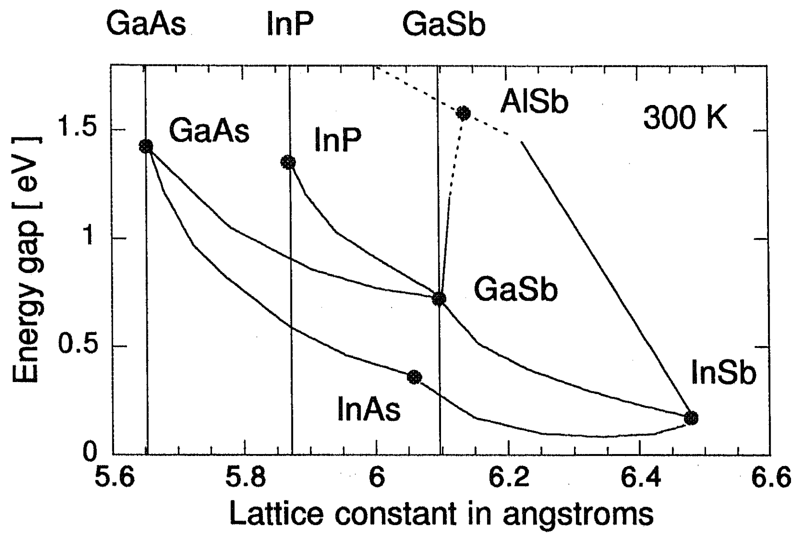

Fig. 1.1: The bandgap at 300 K as a function of the lattice constant for some semiconductors of GaSb and related materials. The lines represent alloys with solid and dashed lines denoting direct at the Γ point and indirect gap at the X point semiconductors, respectively.

the coexistence of electrons and holes across the two interfaces. Bastard *et al.*[27] performed self-consistent calculations for the electronic properties of the quantum wells, predicting the existence of a semiconductor to semi-metal transition as a result of in the GaSb/InAs superlattices. This transition was confirmed by experiments carried out by Munakata *et al.* [28].

Therefore, semiconductor heterointerfaces exhibit an abrupt discontinuity in the local band structure, usually associated with a gradual band bending in its neighborhood which reflects space charge effects. According to a literature[29], such discontinuities can be classified into four kinds: type-I, type-II misaligned, type-II staggered, and type-III as shown in Fig. 1.2.

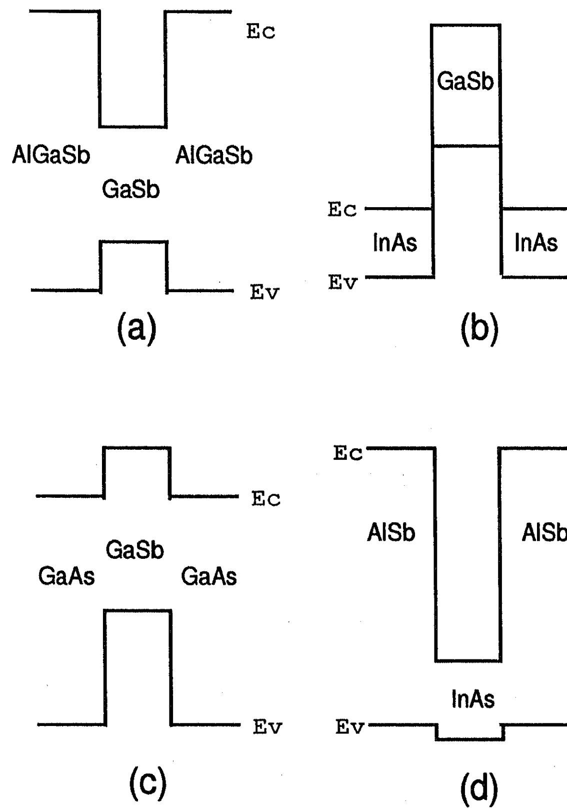

Fig. 1.2: Discontinuities of band edge energies at four types of heterointerfaces: (a) Type-I, (b) type-II misaligned, and (c)(d) type-II staggered band alignment. Ec refers to the conduction band, and Ev to the valence band in real space.

When two materials are joined to form heterostructures, band lineups arising from energy considerations can result in a lower potential for both electrons and holes created in one material (a type-I system in Fig. 1.2 (a)) or a lower potential created for electrons in one material and for holes in the other material (a type-II system in Fig 1.2 (b)-(d)). Figure 1.2 shows a schematic band diagram of the valence and the conduction bands. two semiconductors.

The type-I system in Fig. 1.2 (a) can be considered to be direct in real space, while type-II system in Fig. 1.2 (b)-(d)are indirect, in analogy with band-structure terminology.

- In AlGaSb/GaSb as shown in Fig. 1.2 (a), both electrons and holes are essentially confined in the GaSb (type-I). The AlGaSb/GaSb multilayers grown by MBE have been already used in lasers[30] and photo-conductive detectors[31]. The laser at 1.66 μm realized using this heterostructure. The laser diode continuously operated at room temperature. Excitons were also observed at room temperature[32].

- In InAs/GaSb as shown in Fig. 1.2 (b), The InAs/GaSb system [23, 24, 25] was investigated because of its extraordinary band edge relationship at the interface, called type-II misaligned band alignment, for the first time by Esaki *et al.*

- In GaAs/GaSb as shown in Fig. 1.2 (c), the GaSb layer is a barrier for electrons and a well for holes (type-II). However, the lattice mismatch is 7.8 %. In particular, the GaAs/GaSb quantum dots are described in this thesis.

- In AlSb/InAs as shown in Fig. 1.2 (d), (d) electrons are confined in the InAs layer, holes in the AlSb layer (type-II). This structure is thus a type-II quantum well, inverted with respect to (c). The AlAs/InAs heterostructure offers the combination of a low effective mass for the InAs quantum well ($m^* = 0.023m_e$) and a large conduction band offset (ΔE_c = 1.35 eV). Therefore, it has two attractive properties: (i) it has high mobility over 28,000 cm^2/Vs at room temperature[33] (ii) it has a possibility of an interband transition at 1.55 μm. It allows a promising for novel performance optical and electrical applications.

In addition, either interface bond of InSb or AlSb was selectively made by controlling the beam supply sequence during growth[34].

1.3 Device Applications of GaSb

For optical communication

Optical communication systems in the next generation could be operated above 1.55 μm, even though the present day optical communication systems are tuned to 1.55 μm. This is because recent developments in the optical fiber research have shown potentiality for certain classes of non-silica fibers. The loss minima for optical communication fall in the 2 - 4 μm region.[35] For example, the heavy metal fluoride (F) glasses are speculated to have minimum attenuation at 2.55 μm with a loss. The loss in the heavy metal fluoride (F) glasses is one to two orders of magnitude lower than the present silica fiber. At the wavelength, the loss due to a scattering is significantly reduced. Consequently, research on lasers and detectors in the 2 - 4 μm region are required. A GaSb has been attracted as a substrate material for lasers and detectors in the region.

Devices based on GaSb

GaSb-based devices are one of the promising candidates for a variety of military and civil applications in the 2-5 μm. The GaSb based structures have shown potentiality for applications in lasers [see the next paragraph], infrared photo detectors[36, 37, 38] in the 2 - 5 μm region, high frequency devices[39, 41], superlattice with tailored optical and transport characteristics[42], booster cells in tandem solar cells and high efficiency thermophotovoltaic cells[43].

Lasers in 2 - 5 μm

Laser diodes operating between 2.1 and 2.3 μm have been fabricated of InGaAsSb / AlGaAsSb using both double heterostructures and multiple quantum well structures.[44, 45, 46, 47] Laser diodes of InGaAsSb / AlGaAsSb have been demonstrated at room temperature operation up to 2.78 μm with cw power output as high as 10 mW.[48, 49] Furthermore, longer wavelength up to 4.5 μm are expected. InAs/InGaSb superlattice is of great interest for infrared applications[38]. Strained $Ga_xIn_{1-x}Sb$/InAs superlattice exhibiting a high degree of structural perfection have been on GaSb substrates.[50] The lattice mismatch between InAs and $Ga_xIn_{1-x}Sb$ is f = 2.2% for x=0.25. The InAs/InGaSb superlattice has a type-II band alignment. In 1995, laser diodes using this superlattice at 3.2 μm [51] and up to 4.5 μm were realized by D. H. Chow and R. H. Miles *et al.* [52]. In the case of narrow band gap lasers, the radiative recombination is limited due to the suppression of Auger recombination rates. However, *band structure engineering* permits the design of the InAs/InGaSb optoelectronic devices with tunable energy gaps and suppressed nonradiative recombination rates.[53, 54] Also, InAs/InGaSb strained layer superlattice has shown great promise for application in mid wavelength infrared imaging applications.[55, 56]

1.4 Objectives and Scope of Present Works

Quantum dot devices are expected to drastically improve the characteristics of optical devices and yield novel devices. Recently, self-assembled quantum dots have received a great deal of attention for their possible applications in devices such as high efficiency semiconductor lasers and other novel devices. Compared to InAs/GaAs quantum dots, relatively few works for GaSb/GaAs quantum dots have been reported. However, this system is very attractive from a fundamental

physics point of view and for the possibility of novel device applications. GaSb/GaAs quantum dots should exhibit a type-II band alignment in real space. In this case, holes are localized within the GaSb quantum dots, while due to Coulomb attraction the electrons form a shell around the quantum dots. This system therefore allows the study of semiconductor artificial atoms. In addition, the radiative lifetimes for these type-II quantum dots are longer than those for type-I quantum dots such as InAs/GaAs quantum dots. GaSb/GaAs type-II quantum dots with their long lifetime should be more useful than type I quantum dots for optical memories.

In oder to clarify the characteristics of GaSb quantum dots, there are two objectives:
(i) The first objective of this research is to fabricate GaSb self-assembled quantum dots on GaAs with nano-scale size. It was difficult to control between As and Sb by MBE. However, this problem is overcome by using a valved cracker cell for As and an observation of surface reconstruction. Epitaxial growth of GaSb quantum dots on a GaAs will be established. In such a heterostructure, optical properties are strongly affected by the interface. The structural properties will be investigated not only by atomic force microscopy but also by photoluminescence.

(ii) The second objective of this research is to investigate optical properties of GaSb quantum dots in GaAs, which has type-II band alignment. Some physical properties of the zero-dimensional effects in type-II band alignment will be systematically investigated. Therefore, the type-II staggered band alignment will be confirmed and investigated by measuring photoluminescence, photoluminescence excitation, time-resolved photoluminescence, and photoluminescence in a magnetic field. It will be discussed in terms of physics. These results allow *band structure*

engineering in quantum dots. In addition, type-I InAs and type-II GaSb coupled quantum dots, and InSb dots on GaSb be also investigated.

1.5 Synopses of Chapters

In this thesis, epitaxial growth of self-assembled GaSb quantum dots by molecular beam epitaxy and their optical properties were investigated, in order to realize band engineering in quantum dots and aim novel optical devices. This thesis is organized as follows :

In chapter I, the background of the present study is described on quantum dots, self-assembled quantum dots structures, and band alignment. The aim of this thesis is also given.

In chapter II, epitaxial growth of self-assembled GaSb/GaAs quantum dots is described. In particular, growth condition, growth mechanism, the density control of quantum dots, the stacked structures are discussed.

In chapter III, photoluminescence of GaSb/GaAs quantum dots is described. In particular, photoluminescence reveals not only optical properties but also the structural properties in terms of control of As and Sb in GaSb/GaAs heterostructures. Furthermore, the type-II staggered band alignment is confirmed by the excitation intensity dependence of photoluminescence and theoretical calculation. In addition, temperature dependence of photoluminescence and photoluminescence excitation spectrum are performed. Some physical properties are well investigated. Photoluminescence of stacked structures of GaSb/GaAs Quantum Dots

In chapter IV, time-resolved photoluminescence of GaSb/GaAs quantum dots is described. In particular, lifetimes of GaSb/GaAs quantum dots are systematically

investigated. In addition, the conduction band offset is discussed.

In chapter V, magneto-photoluminescence of GaSb/GaAs quantum dots is described. Photoluminescence measurements in magnetic fields are performed. Diamagnetic shifts and oscillator strength are discussed. In addition, the exciton binding energy are theoretically calculated.

In chapter VI, type-I InAs and type-II GaSb coupled quantum dots are described. Photoluminescence measurements on InAs-GaSb coupled quantum dots are performed. The excitation intensity dependence of photoluminescence measurements reveals the coupled effects between each quantum dots.

In chapter VII, InSb/GaSb self-assembled quantum dots are described. The growth of GaSb buffer layer with a superlattice on a GaAs are performed. The surface morphology is investigated. Furthermore, epitaxial growth of InSb/GaSb quantum dots is performed.

Finally, in chapter VII, conclusions of our main results are described.

Chapter	Contents
I	Introduction
II	Epitaxial Growth
III	Photoluminescence
IV	Time-resolved Photoluminescence
V	Magneto-photoluminescence
VI	Coupled Quantum Dots
VII	InSb Dots and GaSb Buffer Layers
VIII	Conclusions

Table 1.3 : Topics of each chapters in this thesis.

Bibliography

[1] L. Esaki and R. Tsu, IBM Research Note RC-2418 (1969).

[2] L. Esaki and R. Tsu, IBM J. Res. Develop (1970).

[3] Y. Arakawa and H. Sakaki, Appl. Phys. Lett. **40**, 939 (1982).

[4] M. Asada, Y. Miyamoto, and Suematsu, IEEE J. Quantum Electron. **22**, 1915 (1986).

[5] N. Kirstaedter, N. N. Ledentsov, M. Grundmann, D. Bimberg, V. M. Ustinov, S. S. Ruvimov, M. V. Maximov, P. S. Kop'ev, Zh. I Alferov, U. Richter, P. Werner, U. Gösele, and J. Heydenreich, Electron. Lett. **30** 1416 (1994).

[6] H. Shoji, K. Mukai, N. Ohtsuka, M. Sugawara, T. Uchida, and H. Ishikawa, IEEE Photon. Technol. Lett. **12** 1385 (1995).

[7] H. Shoji, Y. Nakata, K. Mukai, Y. Sugiyama, M. Sugawara, N. Yokohama, and H. Ishikawa, Electron Lett. **32** 2023 (1996).

[8] C. W. Snyder, B. G. Orr, D. Kessler, L. M. Sander, Phys. Rev. Lett. **66**, 3032 (1991).

[9] D. Leonard, K. Pond, and P. M. Petroff, Phys. Rev. B. **50**, 11687 (1994).

[10] N. Stranski and L. Krastanow, Sitzungsber. Akad. Wiss. Wien Math. Naturwiss. K1 Abt. 2B Chemie **146**, 797, (1937)

[11] L. Goldstein, F. Glas, J. Y. Marzin, M. N. Charasse, and G. LeRoux, Appl. Phys. Lett. **47** 1099,(1985).

[12] J. Oshinowo, M. Nishioka, S. Ishida, and Y. Arakawa, Appl. Phys. Lett.**65** 1421 (1994).

[13] M. C. Harris Liao, Y. H. Chang, Y. F. Chen, J. W. Hsu, J. M. Lin, and W. C. Chou, Appl. Phys. Lett.**70** 2256 (1997).

[14] M. Kobayashi, S. Nakamura, K. Wako, A. Yoshikawa, K. Takahashi, J. Vac. Sci. Technol. B **16**, 1316, (1998).

[15] P. Schittenhelm, M. Gail, G. Abstreiter, Journal of Crystal Growth **157** 260 (1995).

[16] A. Fissel, K. Pfennighaus, and W. Richter, Appl. Phys. Lett.**71** 2981 (1997).

[17] M. Sopanen, H. Lipsanen, and J. Ahopelto, Appl. Phys. Lett.**67** 3768 (1995).

[18] Xu-Q. Shen, S. Tanaka, S. Iwai, and Y. Aoyagi, Appl. Phys. Lett.**72** 344 (1998).

[19] T. Utzmeier, P. A. Postigo, J. Tamayo, R. Garcica, and F. Briones, Appl. Phys. Lett.**69** 3827 (1996).

[20] B. R. Bennett, R. Magno, and B. V. Shanabrook, Appl. Phys. Lett.**68** (1996) 505.

[21] M. Yano, Y. Seki, H. Ohkawa, K. Koike, S. Sasa and M. Inoue, Jpn. J. Appl. Phys. **37** (1998).

[22] C. H. Casey, Jr. and M. B. Panish, *Heterostructure Lasers, Part A, Fundamental Principles and Part B, Material and Operating Characteristics* Academic Press, New York, 1978.

[23] G. A. Sai-Halasz, R. Tsu, and L. Esaki, Appl. Phys. Lett. **30**, 651 (1977).

[24] G. A. Sai-Halasz, L. Esaki, and W. A. Harrison, Phys. Rev. B **18**, 2812 (1978).

[25] L. L. Chang, N. J. Kawai, G. A. sai-Halasz, R. Ludeke, and L. Esaki, Appl. Phys. Lett. **35**, 939 (1979).

[26] Y. Guldner, J. P. Vieren, P. Voisin, M. Voos, L. L. Chang, and L. Esaki, Phys. Rev. Lett. **45**, 1719 (1980).

[27] G. Bastard, E. E. Mendez, L. L. Chang, and L. Esaki, J. Vac. Sci. Technol. **21**, 531 (1982).

[28] H. Munekata, E. E. Mendez, Y. Iye, and L. Esaki, surf. Sci. 174, **449** (1986).

[29] G. Bastard, "Wave Mechanics Applied to Semicinductor Heterostructures", Les Editions de Physique.

[30] Y. Ohmori, Y. Suzuki, and H. Okamoto, Jpn. J. Appl. Phys. **23** L657 (1985).

[31] R. J. Malik, J. P. Van der Ziel, B. F. Levine, C. G. Bethea, and J. P. Walker, J. Appl. Phys. **59**, 3909 (1986).

[32] T. Miyazawa, S. Tarucha, Y. Ohmori, Y. Suzuki, and H. Okamoto, Jpn. J. Appl. Phys. **25** L200 (1986).

[33] G. Tuttle, H. Kroemer, and J. H. English, J. Appl. Phys. **65**, 5239 (1989).

[34] M. Yano, M. Okuizumi, Y. Iwai, and M. Inoue, J. Appl. Phys. **74**, 7472 (1993).

[35] Special Issue on Low Loss Fibers, IEEE Lightwave Technol. **LT-2** (1984).

[36] O. Hildebrad, W. Kuebart, and M. H. Pilkuhn, Appl. Phys. Lett. **37**, 801 (1980).

[37] S. R. Kurtz, G. G. Osbourn, R. M. Biefield, L. R. Dawson, and H. J. Stein, Appl. Phys. Lett. **52**, 831 (1988).

[38] D. H. Chow, R. H. Miles, J. N. Schulman, D. A. Collins, and T. C. McGill, Semicond. Sci. Technol. **6**, C47 (1991).

[39] K. Segawa, H. Miki, M. Otsubo, and K. Shirata, Electron Lett. **12**, 124 (1976).

[40] S. J. Eglash, H. K. Choi, and G. W. Turner, J. Cryst. Growth **111**, 669 (1991).

[41] C. Hilsum and H. D. Rees, Electron Lett. **6**, 277 (1970).

[42] L. Esaki, J. Cryst. Growth **52**, 277 (1981).

[43] L. M. Frass, G. R. Girard, J. E. Avey, B. A. Arau, V. S. Sundaram, A. G. Thompson, and J. M. Gee, J. Appl. Phys. **66**, 3866 (1989).

[44] G. W. Turner, H. K. Choi, D. R. Calawa, J. P. Pantano, and J. W. Chludzinski, J. Vac. Sci. Technol. **B 12** 1266 (1994).

[45] H. K. Choi and S. J. Eglash, Appl. Phys. Lett. **61**, 1154 (1992).

[46] S. J. Eglash and H. K. Choi, Appl. Phys. Lett. **57**, 1292 (1990).

[47] S. J. Eglash H. K. Choi, and G. W. Turner, J. Cryst. Growth **111**, 669 (1991).

[48] H. Lee, P. K. York, R. J. Menna, R. U. Martinelli, D. Z. Garbuzov, S. Y. Narayan, and J. C. Connolly , Appl. Phys. Lett. **66**, 1942 (1995).

[49] H. K. Choi, and S. J. Eglash, Appl. Phys. Lett. **59**, 1165 (1991).

[50] R. H. Miles, D. H. Chow, and W. J. Hamilton, J. Appl. Phys. **71**, 211 (1992).

[51] R. H. Miles, D. H. Chow, Y. -H. Zhang, P. D. Brewer, and R. G. Wilson, Appl. Phys. Lett. **66**, 1921 (1995).

[52] D. H. Chow, R. H. Miles, T. C. Hasenberg, A. R. Kost, Y, -H, Zhang, H. L. Dunlop, and L. West Appl. Phys. Lett. **67**, 3700 (1995).

[53] C. H. Grein, P. M. Young, and H. Ehrenreich, Appl. Phys. Lett. **76**, 1940 (1994).

[54] C. H. Grein, P. M. Young, and H. Ehrenreich, Appl. Phys. Lett. **61**, 2905 (1992).

[55] D. L. Smith and C. Mailhiot, J. Appl. Phys. **62**, 2545 (1987).

[56] D. H. Chow, R. H. Miles, J. R. Söderström, and T. C. McGill, Appl. Phys. Lett. **56**, 1418 (1990).

Chapter 2

Epitaxial Growth of Self-assembled GaSb/GaAs Quantum Dots

2.1 Introduction

Recently, quantum dots (QDs) have received a great deal of attention for their possible applications in optoelectronic devices such as high efficiency semiconductor lasers [1] as well as for their interesting physical properties. Compared to InAs/GaAs quantum dots, relatively few works for GaSb/GaAs quantum dots have been reported. Unlike for InAs/GaAs QDs, two different group V elements are involved : As and Sb. Table 2.1 shows some lattice constants. The lattice mismatch in the GaSb/GaAs system (7.8%) is close to that in the InAs/GaAs system (6.9%). The formation of GaSb/GaAs QD by molecular beam epitaxy (MBE) in the Stranski-Krastanow (S-K) growth mode have been reported [2, 3, 4]. However, detailed discussion of the optimized growth conditions in the Stranski-Krastanow growth mode has not been established. So far, GaSb/GaAs QDs with diameters in the 10 - 20 nm region, and systematic density control have not been reported.

In this chapter, we describe the fabrication of a GaSb/GaAs quantum-sized dots (~25nm) by the Stranski-Krastanow growth mode of MBE. Reflection high-energy electron diffraction (RHEED) reveals information regarding the growth procedure and the growth mechanism.[5] Consequently, control of dot density is systematically obtained by carefully choosing the amount of deposited GaSb. Also, the details regarding growth procedure is discussed. In addition, stacked structures of the GaAs/GaSb quantum dots are grown.[6]

Materials	GaAs	GaSb	AlSb	InAs	InSb	InP
Lattice a (Å)	5.65325	6.09593	6.1355	6.0583	6.47937	5.8687

Table 2-1 : Lattice parameters in several materials.

2.2 Epitaxial Growth Conditions

Molecular beam epitaxy

In order to fabricate the GaSb/GaAs QDs the samples were grown by solid source molecular beam epitaxy (VG80H Mark MK-III). As it is necessary to change from As to Sb a valved cracker cell for As_2 (EPI-500As) was used which should suppress the unintentional inclusion of As resulting in an alloy GaSbAs[7]. The Sb source was used uncracked molecular Sb_4. The beam intensities were monitored by a nude ion gauge at the substrate position before the growth. The deposition was monitored *in situ* by RHEED during the growth.

This VG80 MBE chamber can produce high quality films. For example, two-

dimensional electrons of an AlGaAs/GaAs single structure exhibited the electron mobilities $\mu = 150{,}000\ cm^2/Vs$ at 77K under light. Therefore, we expect the unintentional doping level of the GaAs layers was as low as $10^{14} - 10^{15}\ cm^{-3}$. Furthermore, the high mobility was obtained, even though after an Sb was used.

A valved cracker cell for As

There are problems in a conventional As effusion cell :

(1) it is keep to have a stable As flux with a effusion cell.

(2) it is impractical to raise and lower the As effusion cell temperature with a short period of time due to the large mass of As cell. It means difficult to control As flux.

In order to control high pressure As, the valved cracker cell for As_2 (EPI-500As) was used. It allows to change from As to Sb, which should suppress the unintentional diffusion. Epitaxial growth of high structural quality GaInSb/InAs superlattice using a cracker cell [7] has been reported previously. Therefore, we employed a valved cracker cell (EPI-500As) for As_2 to control the change from high pressure As to Sb. On the other hand, a conventional cell for Sb_4 was used.

Epitaxial growth procedure of GaSb quantum dots on a GaAs (001)

Figure 2.1 shows a schematic diagram of the growth procedure. After oxide desorption, a GaAs buffer of approximately 250-nm-thick was grown at 580°C on a GaAs semi-insulating (001) substrate. The growth rate was 0.74 mono-layer (ML) /s under As_2 1.8×10^{-5} Torr. The RHEED pattern exhibited a fine streak (2×4)

reconstruction. In order to use slower growth rate and low pressures of As and Sb for the deposition of the QDs, it is necessary to reduce the Ga flux. The Ga flux was slowly decreased to 1.6x10^{-7} Torr within 20 minutes during the GaAs buffer growth. After the Ga cell temperature stabilized, growth was interrupted under As_2 for 5 minutes. The substrate was then cooled down to a temperature of 450°C. During the growth interruption, the As_2 pressure was also reduced to 2.0x10^{-6} Torr using the valve. At this point the RHEED indicated that the GaAs surface was a c(4×4) reconstruction. The Sb_4 was set at 8.0x10^{-7} Torr giving a Sb_4/Ga flux ratio of 5.

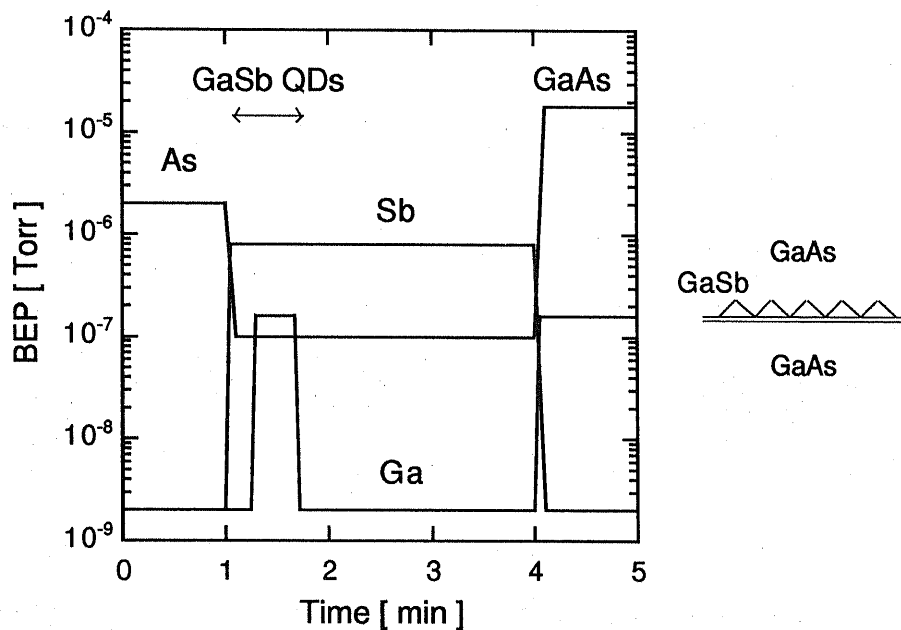

Fig. 2.1: A schematic diagram of the growth procedure for GaSb/GaAs quantum dots. The inset shows a drawing of sample structure.

Firstly, the valve and the shutter for As were closed. The substrate was then irradiated with Sb_4. After 5 seconds the As_2 pressure was measured to be reduced by

one order of magnitude. After 15 seconds the RHEED pattern changed to a (1×3) reconstruction indicating a GaSb surface. This means that 1 ML GaSb exists on the surface (although no gallium was deposited). Following this pause of 15 seconds GaSb was grown at 0.086 ML/s. During the deposition the growth changed when a total of 2.5 ML was deposited from 2 D to 3 D indicated by the appearance of a spotty RHEED pattern. After the growth, the surface was kept for 140 seconds at the same temperature, and finally cooled under an Sb_4 flux.

On the other hand, the GaSb quantum dots were capped by a GaAs layer for photoluminescence measurements. The GaAs cap layer was grown using the same temperature and the same growth rate as were used for the QDs. This was to avoid the possibility of destroying the QDs through intermixing of As and Sb. During the growth of this GaAs cap layer, the RHEED pattern gradually recovered to a c(4×4) reconstruction.

2.3 Discussion on the Epitaxial Growth Conditions

Surface reconstruction

In this study RHEED has revealed a variety of surface reconstruction which correlate with the grown process. Figure 2.2 shows a schematic drawing of the growth mechanism on the surface.Initially the GaAs (001) As-stabilized c(4×4) reconstruction is observed at 450°C under As_2. The surface consists of As-As ad-atom. Following the irradiation of the GaAs surface with Sb_4 8.0×10^{-7}Torr, within 15 seconds the surface was changed from As terminated to Sb terminated. This was evidenced by a change in the RHEED pattern to a Sb-stabilized (1×3) reconstruction from the c(4×4) GaAs surface. The first 1ML of GaSb is formed due to the

exchange of As and Sb. A spotty pattern appeared after the deposition of a total of 2.5 ML of GaSb due to three dimensional growth.

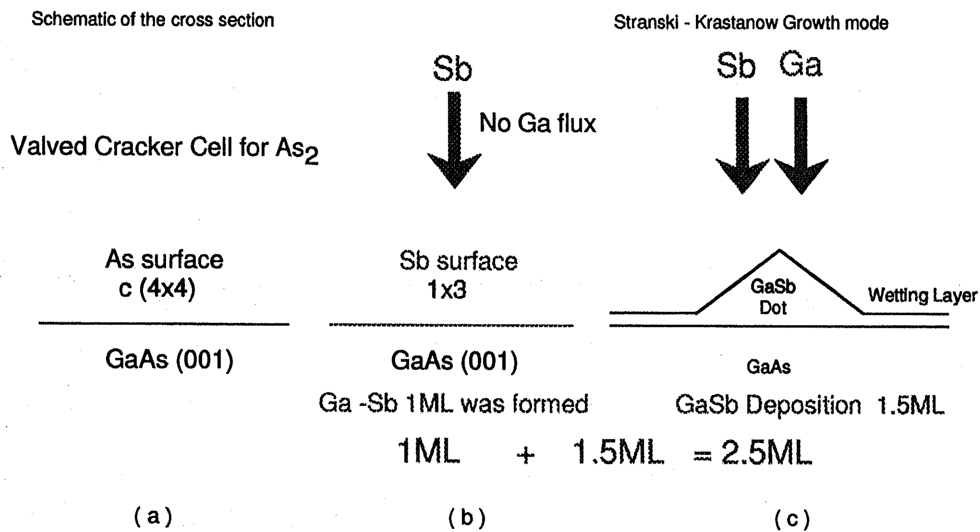

Fig. 2.2: A schematic drawing of the growth mechanism on the surface.

Similar results support this RHEED transition from a c(4×4) to to a (1×3). This reconstruction indicates a GaSb surface[8, 9, 10]. This means that 1 ML GaSb existed on the surface (although no gallium was deposited). Furthermore, we should discuss another method regarding this reaction. N. N. Ledentsov *et al.* investigated structural properties using a double-crystal x-ray diffractometer.[11] According to the report, the 10 s growth interruption under Sb_4 flux performed after GaAs deposition in a GaSb/GaAs have shown that the effective width of the GaSb layers formed under these conditions equals 0.317 nm. Thus it was concluded that a complete GaSb monolayer forms at 470 °C with in 10 s under Sb flux. Formation of a second GaSb monolayer occurs within an additional 15 - 20 s. Further increase of growth interruption time does not result in a significant increase of GaSb layer thickness.

Therefore, we conclude that these comparison support the exact formation of 1 ML of GaAs after the exposure of GaAs surface to an Sb flux, and the thickness of the wetting layer is 2 ML. In addition, photoluminescence measurements also reveal it in chapter III.

The Sb/Ga ratio

A laser using AlGaAs/GaSb heterostructures has been reported[12]. The laser was operated by current injection at room temperature. Then the flux ratio of Sb/Ga was kept around 2 to obtain mirror surface and high photoluminescence intensity. It suggests that growth condition at the low Sb/Ga can grow high quality films. In our experiments, the result is also available for the GaSb quantum dots. A high Sb pressure is expected to suppress Ga migration, and exchange rapidly from As to Sb terminated on GaAs. It is therefore important to maintain the Sb flux as low as possible. With the low Sb_4/Ga ratio, the dot diameter can became more uniform. As a consequence of this, we optimized the Sb_4/Ga ratio of GaSb QD at 5.

The Epitaxial Growth temperature

At the lower temperature, it is not sufficient for deposited atoms to form the QDs uniformly due to the lower surface energy. As the substrate temperature is increased, however, it is unintentionally incorporated resulting in a GaSbAs layer [13, 14]. In order to strike a balance between the two, we selected a growth temperature for the GaSb QDs of 450°C.

An alloy GaSbAs and a miscibilty gap

In spite of the large miscibility gap of $GaAs_xSb_{1-x}$ alloys, stable epitaxial GaAsSb ordered structures[15] and epitaxial GaAsSb disordered alloys[16] have been grown well inside the miscibility gap. The composition of alloyed crystals such as GaSbAs has been shown to be strongly dependent on the growth conditions, particularly on the substrate temperature and the arrival rates of As and Sb molecules [13]. On the other hand, it has been known that the predominant incorporation of Sb is reduced with increasing growth temperature [13, 14]. In our experiments, the optimum growth conditions for GaSb QDs suppressed the formation of the alloy GaSbAs.

The Kinetic barrier

The lattice mismatch seems to be unimportant in determining the diameter of the dots. If it were the dominant factor, one would expect similar result to those obtained for InAs/GaAs QDs due to the very similar lattice mismatch between InAs/GaAs and GaSb/GaAs. On the other hand, the binding energy of Ga-Sb and In-As is different[9] and the migration is different between Ga and In. As there is a kinetic barrier to clustering in the S-K growth mode the InAs QDs and the GaSb QDs on a GaAs should have different growth mechanisms.

2.4 Density Control of Quantum Dots

All samples were characterized using atomic force microscopy (AFM) by Digital Instruments Nanoscope. Figure 2.3 shows AFM images ($1\mu m \times 1\mu m$) of the as-grown surface observed at the room temperature and atmosphere.

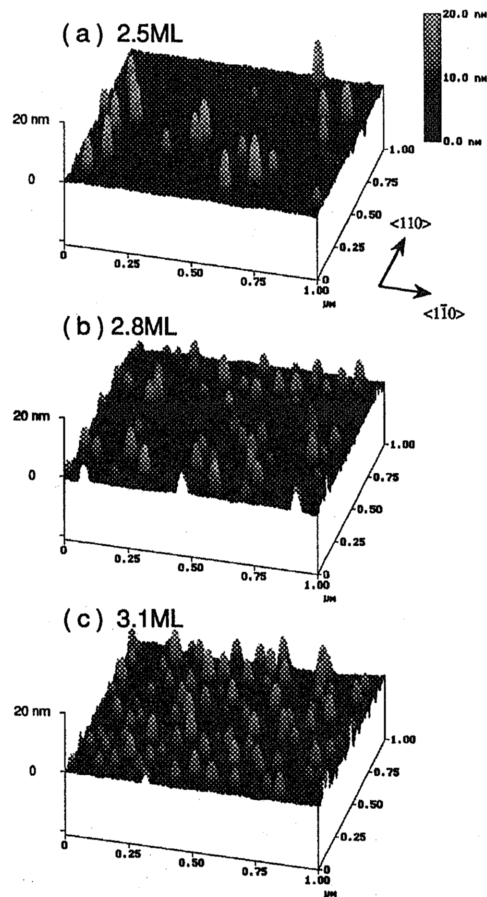

Fig. 2.3: AFM images (1μm $\times$ 1μm) of the GaSb quantum dots on a a GaAs surface for (a)2.5ML, (b)2.8ML,and (c)3.1ML deposited. The others parameter were fixed except the amount of deposition.

The amount of deposited material was varied while keeping all other parameters fixed. Following the deposition of a total of 2ML of GaSb, the surface remained relatively flat. After a critical deposition thickness was achieved, the surface was transformed into three-dimensional as evidenced by the spotty pattern of RHEED.

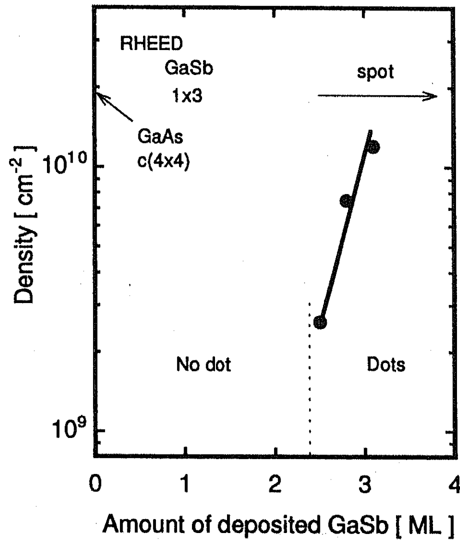

Fig. 2.4: Dependence of QD Densities on amount of deposited GaSb. The insert shows the RHEED pattern during the growth.

The quantum dots were obtained by the deposition of 2.5ML of GaSb are shown in Fig. 2.4 (a).

In this case, the deposition of 2.5ML means the first 1ML of Sb terminated on the surface due to the Sb irradiation before the deposition of 1.5ML of GaSb. In addition, Fig. 2.3(b) and (c) show AFM images for 2.8ML and 3.1ML of deposited GaSb. The densities are $2.6\times10^{9}cm^{-2}$, $7.5\times10^{9}cm^{-2}$, and $1.2\times10^{10}cm^{-2}$ for (a)2.5ML, (b)2.8ML, and (c)3.1ML, respectively. It is clear that the densities were systematically changed by carefully choosing the amount of deposited GaSb at these optimized growth conditions. Here our measurements are limited by the shape of the AFM tip, so that actual lateral diameters of the QDs are smaller than the values given above.

Histograms of the GaSb QD diameter which are fitted with a Gaussian curve are indicated. The diameter (d) and the average height (h) were d = 32±5 nm h = 9.5 nm, d=28±6nm h = 6.7 nm, and d = 26±6 nm h=6.2 nm for the total deposition of 2.5 ML, 2.8 ML, and 3.1 ML, respectively. As the deposition is increased; the density drastically increased, the height is reduced, and quite remarkably smaller QDs appear to be formed. Figure2.4 shows a plot indicating the RHEED pattern and dot density versus the amount of GaSb deposited.

Facets

We should discuss the shape of the GaSb quantum dots. The values determined by AFM section analyses are in good agreement with the theoretical value $\Theta_{113} = 25°$ rather than $\Theta_{111} = 54°$. Eaglesham *et al.* considered the {113} facet to be the equilibrium shape in quantum dot structures[17]. It has in a good agreement with our results.

The height (~9.5nm) of GaSb QD is considerably taller than that of InAs QD (~3nm). Fluctuations in the height, rather than the diameter of the QDs, are expected to be the dominant factor in the full width of half maximum (FWHM) of photoluminescence (PL). Therefore, one would expect PL with a narrow FWHM from the GaSb QD. It was found experimentally for capped samples [18]. Photoluminescence measurements also reveal it in chapter III.

2.5 Stacked Structures

Recently, stacked structures of InAs/GaAs quantum dots have become possible by molecular beam epitaxy. InAs quantum dots are vertically aligned in columns and pseudomorphic.[19, 20, 21] Lasing characteristics of InAs/GaAs stacked structures also have been realized.[22] However, the stacked structures of GaSb/GaAs have not yet been reported. One reason is the difficulty of control the growth of GaSb/GaAs heterostructures.

In this work, we report growth of GaSb/GaAs coherent quantum-sized QDs using a valved cracker cell for As, which allows good control of the switching between supplying As and supplying Sb despite the deposition of only a few monolayers. In particular, we grow the stacked structure of self-assembled GaSb QDs on a GaAs by MBE. We characterize the surfaces by atomic force microscopy.

Epitaxial growth procedure for stacked structure.

The stacked structures of self-assembled GaSb/GaAs QDs were grown by the following growth procedure. A GaAs buffer layer, approximately 300 nm thick, was grown at 580 °C on a GaAs semi-insulating (001) substrate. The RHEED pattern exhibited a (2×4) reconstruction. The growth rate was 0.74 ML/s , and the beam equivalent pressure (BEP) of As_2 was 1.8×10^{-5} Torr. In order to use a slower growth rate and lower pressure of As and Sb for the deposition of the QDs, it is necessary to reduce the Ga flux. The Ga BEP was slowly decreased to 1.6×10^{-7} Torr over 20 minutes during the growth of the GaAs buffer layer. The growth rate was set at 0.086 ML/s for the QDs. After the Ga cell temperature stabilized, the

growth was interrupted under As_2 for 5 minutes. The substrate was then cooled down to 450 °C for the formation of the self-assembled QDs.

During the growth interruption, the As_2 BEP was also reduced to 2.0×10^{-6} Torr by adjusting the valve. At this point the RHEED indicated a c(4×4) reconstruction. The Sb_4 BEP was set to 8.0×10^{-7} Torr giving a Sb_4/Ga flux ratio of 5. Both the valve and the shutter for As were closed. The substrate was then irradiated with Sb_4. After 5 seconds the As_2 BEP was found to be reduced by an order of magnitude. After 15 seconds, the RHEED pattern changed to a (1×3) reconstruction indicating a GaSb surface [8, 9, 10]. This means that 1 ML GaSb existed on the surface (although no gallium was deposited). A spotty RHEED pattern indicated a change to 3D growth from 2D growth after the deposition of 2.5 ML including the first 1 ML. After the deposition of a total of 3.1 ML, the surface was kept for 140 seconds at the same temperature under an Sb_4 flux. The deposition of 3.1 ML means the first 1 ML of Sb terminated on the surface due to the Sb irradiation (only Sb shutter open) before the deposition of 2.1 ML of GaSb (Ga and Sb shutters open). After the first QDs were formed, an interval GaAs layer, 10 nm thick, was grown using the same Ga flux as for the QDs, and As BEP set at 1.8×10^{-5} Torr. During the growth of this GaAs interval layer, the RHEED pattern gradually recovered to a c(4×4) reconstruction. The growth was interrupted for 1 minute under As BEP of 2×10^{-6} Torr before the QDs of the next layer were grown by same growth procedure as was used for the first layer. By repeating this growth procedure, multi-stacked QDs were obtained. The growth temperature and V/III flux ratio were fixed throughout growth of the stacked structure. Finally the substrate was cooled under an Sb_4 flux.

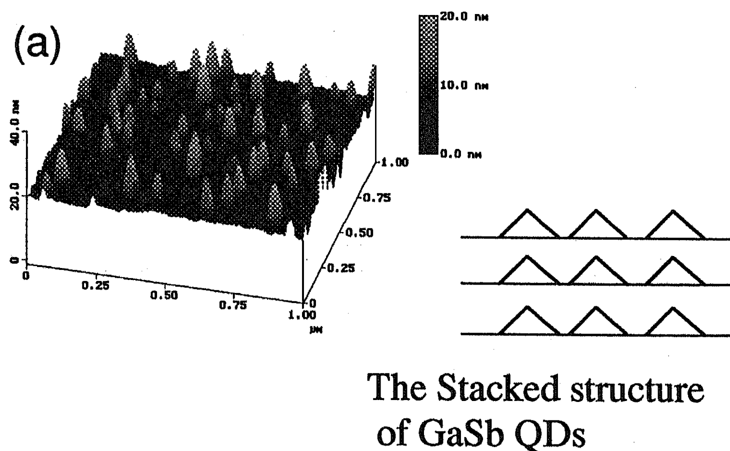

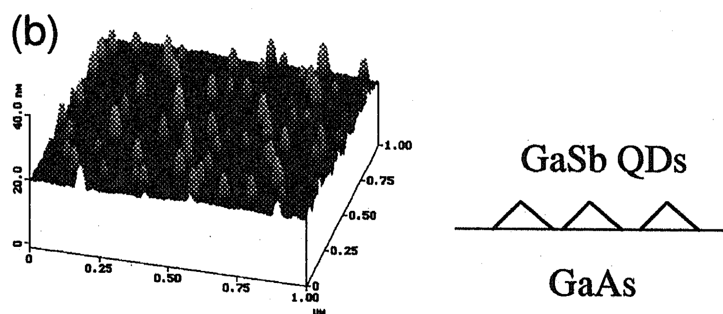

Fig. 2.5: AFM images of the self-assembled GaSb quantum dots on a GaAs. (a) the third layer of a stacked structure and (b) the first layer.

AFM measurements of the stacked structure

The QDs were characterized by AFM. Figures 2.5 (a) and (b) show AFM images (1 μm by 1 μm) of the as-grown surface. Figures 2.5 (a) and (b) are the third and the first layers of un-capped GaSb QDs surfaces, respectively. The QDs of the first and the third layers have diameters $\sim 38 \pm 7$ nm and $\sim 42 \pm 8$ nm, heights ~ 7 nm and ~ 8 nm, and densities 8×10^{10} cm^{-2} and 7×10^{10} cm^{-2}, respectively. We note that the values are similar in the two layers. However, the average diameter of the third layer QDs was 110 % larger than the that of the first layer QDs. These features

correspond well to those observed stacked structures of InAs/GaAs QDs [20]. Here our measurement is limited by the shape of the AFM tip, so that the actual lateral diameter of the QDs must be smaller than that given above.

2.6 Summary

In chapter II, epitaxial growth using the Stranski-Krastanow mode has described the formation of self-assembled GaSb quantum dots on a GaAs. The growth mechanism are also discussed in detail. Consequently, the average diameter and height of the quantum dots are 26nm and 6.2nm, respectively. Moreover, the density was systematically controlled between 2.6x10^{9} to 1.2x10^{10} cm^{-2} by carefully choosing the amount of deposited GaSb from 2.5ML to 3.1ML. In addition, a stacked structure of self-assembled GaSb/GaAs QDs with nanometer-scale dimensions also were grown. These results are very useful in forming a QD of staggered band lineup (type-II) of possible use in novel device applications.

Bibliography

[1] Y. Arakawa and H. Sakaki, Appl. Phys. Lett. **40**, 939 (1982).

[2] F. Hatami, N. N. Ledentsov, M. Grundmann, J. Böhrer, F. Heinrichsdorff, M. Beer, D. Bimberg, S. S. Ruvimov, P. Werner, U. Goesele, J. Haydenreich, U. Richter, S. V. Ivanov, B. Ya. Meltser, P. S. Kop'ev, and Zh. I. Alferov, Appl. Phys. Lett.**67** (1995) 656.

[3] C. -K. Sun, G. Wang, J. E. Bowers, B. Brar, H. -R. Blank, H. Kroemer, and M. H. Pilkuhn, Appl. Phys. Lett. **68** (1996) 1543.

[4] B. R. Bennett, R. Magno, and B. V. Shanabrook, Appl. Phys. Lett.**68** (1996) 505.

[5] K. Suzuki, R. A. Hogg, K. Tachibana, and Y. Arakawa, Jpn. J. Appl. Phys. **37** (1998) L203.

[6] K. Suzuki and Y. Arakawa, *To be published in* Journal of Crystal Growth

[7] R. H. Miles, D. H. Chow, and W. J. Hamilton, J. Appl. Phys. **71** (1992) 211.

[8] R. Ludeke, Phys. Rev. Lett. **39** (1977) 1042.

[9] M. Yano, Y. Yokose, Y. Iwai, and M. Inoue, J. Crystal Growth **111** (1991) 609.

[10] F. Maeda, Y. Watanabe, and M. Oshima, Phys. Rev. B **48** (1993) 14733.

[11] N. N. Ledentsov, J. Böhrer, M. Beer, F. Heinrichsdorff, M. Grundmann, D. Bimberg, S. V. Ivanov, B. Ya. Meltser, S. V. Shaposhikov, I. N. Yassievich, N. N. Faleev, P. S. Kop'ev, and Zh. I. Alferov, Phys. Rev. B **52** (1995) 14058.

[12] Y.Ohomori, S. Tarucha, Y. Horikoshi, and H. Okamoto, Jpn. J. of Appl. Phys. **23** L94 (1984).

[13] M. Yano, M. Ashida, A. Kawaguchi, Y. Iwai, and M. Inoue, J. Vac. Sci. & Technol B**7** (1989) 199.

[14] Chin-An Chang, R. Ludeke, L. L. Chang, and L. Esaki, Appl. Phys. Lett. **31** (1977) 759.

[15] H. R. Jen, M. J. Cherng, and G. B. Stringfellow, Appl. Phys. Lett.**48** 1603 (1986).

[16] R. M. Cohen, M. J. Cherng, R. E. Benner, and G. B. Stringfellow, J. Appl. Phys. **57**, 4817, (1985).

[17] D. J. Eaglesham, F. C. Unterwald, and D. C. Jacobson, Phys. Rev. Lett. **70** 966, (1994).

[18] R. A. Hogg, K. Suzuki, K. Tachibana, L. Finger, K. Hirakawa, and Y. Arakawa, Appl. Phys. Lett. **72** (1998) 2865.

[19] G. S. Solomon, J. A. Trezza, A. F. Marshall, and J. S. Harris,Jr. Phys. Rev. Lett. **76** 952, (1996).

[20] Y. Nakata, Y. Sugiyama, T. Futatsugi, and N. Yokohama, J. Cryst. Growth **175/176** (1997) 713.

[21] Y. Sugiyama, Y. Nakata, T. Futatsugi, M. Sugawara, Y. Awano, and N. Yokohama, Jpn. J. Appl. Phys. **36** L158 (1997).

[22] H. Shoji, Y. Nalata, K. Mukai, Y. Sugiyama, M. Sugawara, N. Yokohama, and H. Ishikawa, Jpn. J. Appl. Phys. **35** L903 (1996).

Chapter 3

Photoluminescence of Type-II GaSb/GaAs Quantum Dots

3.1 Introduction

Quantum dots (QDs) have received a great deal of attention for their possible applications in devices such as high efficiency semiconductor lasers [1]. Compared to InAs/GaAs QDs, relatively few works for GaSb/GaAs QDs have been reported. However, this system is very attractive from a fundamental physics point of view and for the possibility of novel device applications such as optical memories.[2] GaSb/GaAs QDs should exhibit a type-II band alignment in real space.[3-9] In this case, holes are localized within the GaSb QDs, while due to Coulomb attraction the electrons form a shell around the QDs. This system therefore allows the study of semiconductor artificial atoms.

Recently, the formation of GaSb/GaAs self-assembled QDs has become possible by molecular beam epitaxy (MBE) in the Stranski-Krastanow (S-K) growth mode.[4-12] However, the optical properties of the QDs depend strongly on the growth technique. One of the reasons is the difficulty of controlling the growth of GaSb/GaAs heterostructures due to strong As-Sb intermixing [13, 14, 15]. There-

fore, the photoluminescence spectrum had unexpected features.[4, 6, 8, 9] The structural properties of GaSb/GaAs self-assembled quantum dots (QDs) were described in the chapter II. In this chapter, photoluminescence properties of GaSb/GaAs coherent self-assembled QDs are described. There are two purposes to investigate photoluminescence properties:

(1) We can confirm whether GaSb/GaAs quantum dots was grown by photoluminescence measurements.

(2) We can investigate intrinsic optical properties of GaSb/GaAs quantum dots. Therefore, a type-II band alignment of the GaSb/GaAs quantum dots are discussed.

Previous reports of the optical properties of these structures[4, 9, 10] have shown photoluminescence (PL) peaks from 1.1 to 1.375 eV attributed to GaSb QDs, however, until now a detailed study incorporating excitation spectroscopy of these structures has not been discussed. Recently, we have reported optimized growth conditions for the growth of GaSb QDs in the chapter II. We report an optical spectroscopic study of these GaSb/GaAs QDs. We unambiguously identify luminescence due to the QDs and show the dependence of the PL spectra upon the excitation conditions. In addition, features observed in photoluminescence excitation spectrum are discussed in terms of phonon relaxation.

3.2 Photoluminescence

The Stranski-Krastanow growth mode allows the realization of quantum dots of high optical quality, and has been of considerable recent interest[16, 17, 18, 19]. The GaSb/GaAs system exhibits a type II band-alignment. GaSb forms a well for holes but a barrier for electrons. Type II QDs should exhibit a number of interesting

properties such as a large tunability of the emission energy and a dependence of the oscillator strength on the QD size[20]. Due to the spatial separation of electrons and holes, the radiative lifetimes for type II QDs should be considerably longer than that for the type I case (e.g. InAs/GaAs).

Sample

Optical properties of GaSb/GaAs QDs depend strongly on the growth technique. It was difficult to control As-Sb intermixing. Therefore, the photoluminescence spectrum had unexpected features.[4, 6, 8, 9] In order to confirm the structure of our QDs, we investigated the PL of the QDs capped by 50 nm thick of GaAs. The sample was capped by 50 nm of GaAs for optical measurements. The GaAs cap layer was grown using the same temperature and the same growth rate as were used for the QDs. This was to avoid the possibility of destroying the QDs through intermixing of As and Sb. During the growth of this GaAs cap layer, the RHEED pattern gradually recovered to a c(4×4) reconstruction.

PL measurements

In order to investigate the optical properties, PL measurements were performed at low temperatures with the sample mounted in a closed-cycle helium cryostat. The sample was excited at various excitation power densities using the 488 nm line (2.54 eV) of an Ar^+ laser. The PL was dispersed by a 50 cm single stage spectrometer and detected using a liquid nitrogen cooled InGaAsP/InP photo multiplier tube (Hamamatsu photonics R5509-41) ,which is sensitive up to 1.4 μm. The excitation was chopped and the signal recovered by standard lock-in techniques.

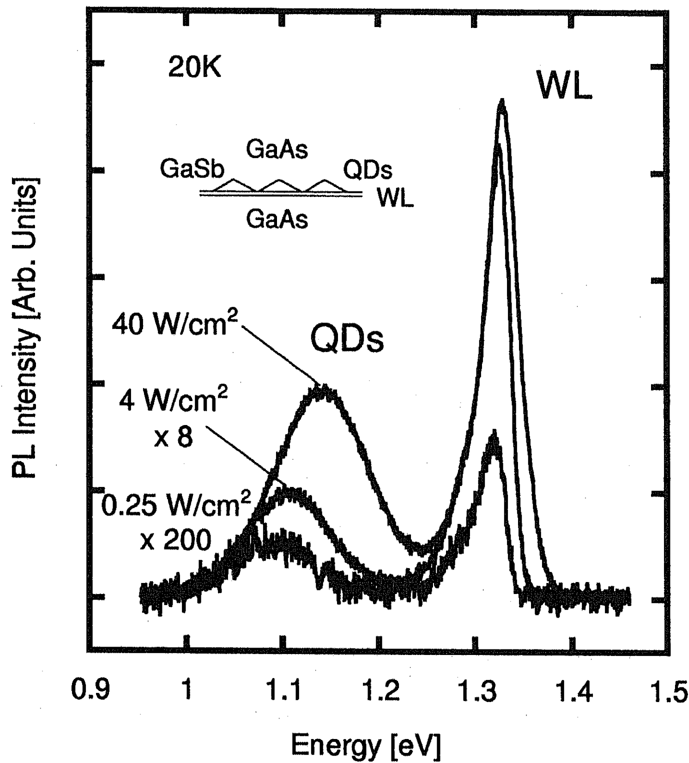

Fig. 3.1: PL spectra of the GaSb/GaAs QDs at different excitation power densities. The PL from the QDs is clearly separated from that of the WL. A blue shift with increasing excitation power is clearly observed.

PL spectrum

The inset of Fig. 3.1 shows the sample structure. Previous PL reports have shown a single peak spectrum [6, 9] or overlapped spectrum from the QDs and a wetting layer (WL) [4, 8]. These reported results mean there are difficulties of switching between As and Sb. However, we clearly observed separated PL peaks from the QDs and the WL, as shown in Fig. 3.1 The full width at half-maximum (FWHM) of spectrum from the QDs and the WL are 100 meV and 37 meV, respectively. We note that there is *no overlap* of the two peaks. Furthermore, the peaks are also sharper than that previously reported [4, 8]. This result indicates that epitaxial

growth of the GaSb/GaAs heterostructure is well controlled without any switching problems despite the deposition of only a few ML. This was achieved by using a valved cracker cell for As ,which allows control of the switching between As and Sb.

Is the wetting layer 2 monolayers ?

We discuss the formation of 1 ML GaSb after the exposure of GaAs surface to Sb flux except for the evidence of the formation of a (1×3) RHEED pattern. We compare with another evidence, in order to support it. There are two evidences: (i) We can compare with a study on structural properties using x-ray. N.N.Ledentsov *et al.* investigated GaSb/GaAs superlattice grown by MBE by using a double-crystal x-ray diffractometer.[15] The detail was described in chapter II. (ii) The other evidence is to compare with the PL emission energy. Previous reports of the optical properties of these structures have shown PL peaks at ~1.3 eV attributed to the GaSb 2 monolayers (ML) quantum well.[15] It is in a good agreement with our data of PL peak at 1.3 eV from 2 ML GaSb as shown in Fig. 3.1. Therefore, we conclude that these comparison support the exact formation of 1 ML of GaAs after the exposure of GaAs surface to Sb flux, and the thickness of the wetting layer is 2 ML.

On the other hand, there is slight disagreement between experimentally observed and theoretically calculated PL energies (1.1 eV) [15]. The reasons are attributed to unknown exact parameters (band offset, effective mass and etc.). However, we note these are quit close values between our data and Ledentsov's data investigated well.

3.3 Excitation Intensity Dependence

Figure 3.1 shows the PL from the capped sample at excitation intensities 40 W/cm^2, 4.0 W/cm^2, and 0.25 W/cm^2. The lower (~1.1 eV) and higher (~1.3 eV) energy features are attributed to the GaSb QDs and the WL, respectively. The peaks due to the QDs and the WL at an excitation of 40 W/cm^2 have full width at half-maximum (FWHM) of 100 meV and 37 meV, respectively. The broadness of the QDs peak is attributed to size fluctuations of the QDs. The FWHM of the WL peak is three times smaller than that of the QDs line.

With increasing excitation intensity, the peak from the QDs shifts towards higher energies as shown in Fig. 3.1. We show a plot of the energies of the QDs and the WL peaks as a function of the excitation power (P) in Fig. 3.2. The observed blue shift is due to the increase of charge within the QDs and a corresponding increase of the sharpness of the Coulomb potential confining the electrons. The effects lead to an increase in the confinement energies for electrons.

The change in emission energy is expected to follow the third root of the excitation density $P^{1/3}$ [4, 8, 15]. [See Appendix A.] The fitted lines in Fig. 3.2 represent $CP^{1/3}$ with different constants (C) and offset energies for the QDs and the WL data. The ratio C_{QDs}/C_{WL} is 6.5. The GaSb/GaAs system should exhibit a staggered (type-II) band alignment [see Fig. 3.2 inset]. In this case, the apparent blue shift of the QDs peak appears to be due to the filling of the QDs levels and the effect of increasing charge density in the QDs. Similar blue shifts have been observed by Hatami *et al.*[4, 8] and C. -K. Sun *et al.*[9] and support the QDs having staggered

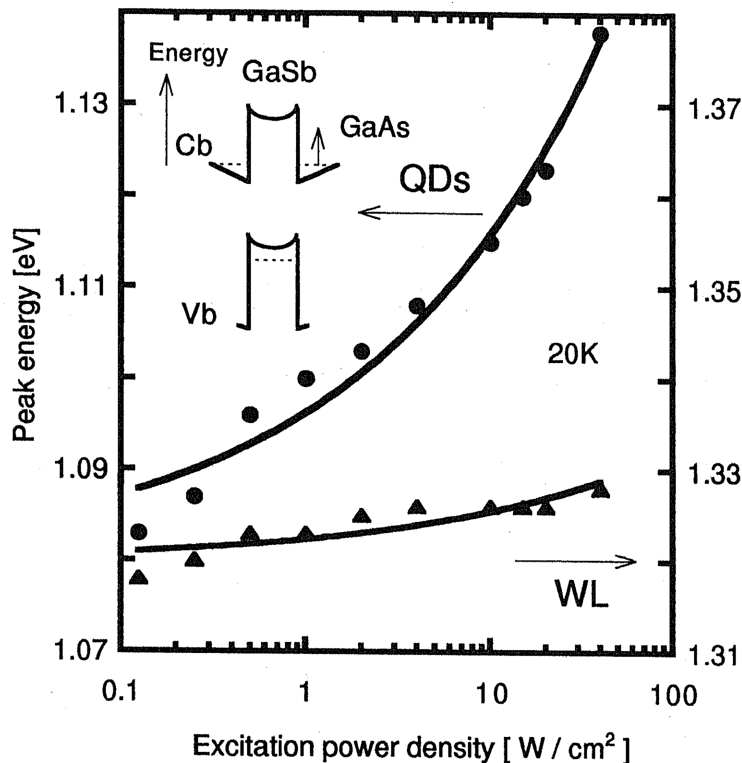

Fig. 3.2: The excitation power dependence of the PL peak energies for the GaSb/GaAs QDs. With increasing excitation intensity, the peak from the QDs shifts towards higher energies. The shift of the QDs peak is 6.5 times larger than that of the WL peak. The blue shift with increasing excitation intensity indicates type-II band alignment. The inset shows a schematic diagram of the conduction and valence bands for type-II band alignment with a band bending effect due to spatially separated charge.

(type-II) band lineup. We note the observed shift of the QDs peak to be 6.5 times larger than that of the WL peak [4, 8]. The Coulomb effects in the QDs and the WL are different.

3.4 Excitation Energy Dependence

2.5 ML QDs and 2 ML (*no dots*)

Using a valved cracker cell and growing GaAs using As_2, we have been able

to optimize the growth conditions for this system, leading to good size uniformity and precise density control of the QDs. A 100nm GaAs buffer layer was grown, and following a 5 second delay with the sample exposed to an Sb flux, 2 monolayers (MLs) or 2.5 ML of GaSb was deposited. For the 2.5 ML, sample the reflection high-energy electron-diffraction (RHEED) pattern showed a spotty pattern indicating 3D S-K growth. Following a growth interruption of 140 seconds under an Sb flux, samples for optical measurements were capped with 50 nm of GaAs. These measurements indicate the formation of QDs of height 8-10 nm, diameter 25-35 nm, and density $2\times10^{9}cm^{-2}$.

Different excitation energies

We identify the QD luminescence obtained at different excitation energies and densities. We show how for these structures not only the spectral position of peaks, but also their relative intensities are critically dependent on the density of photo-generated carriers.

The samples are referred to as 2 ML quantum well (QW) and 2.5 ML samples. PL measurements were carried out at 10 K with the samples mounted in a closed-cycle helium cryostat. PL was excited at various excitation densities using either a frequency doubled Nd:YVO_4 laser at 532 nm (2.33 eV) or a frequency doubled Nd:YVO_4 pumped Ti:Sapphire laser at 840 nm (1.48 eV). The luminescence was dispersed by a 25 cm single stage spectrometer giving a resolution of 3 meV and was detected using a liquid nitrogen cooled InGaAsP photomultiplier tube. The excitation was chopped and the signal recovered by standard lock-in techniques.

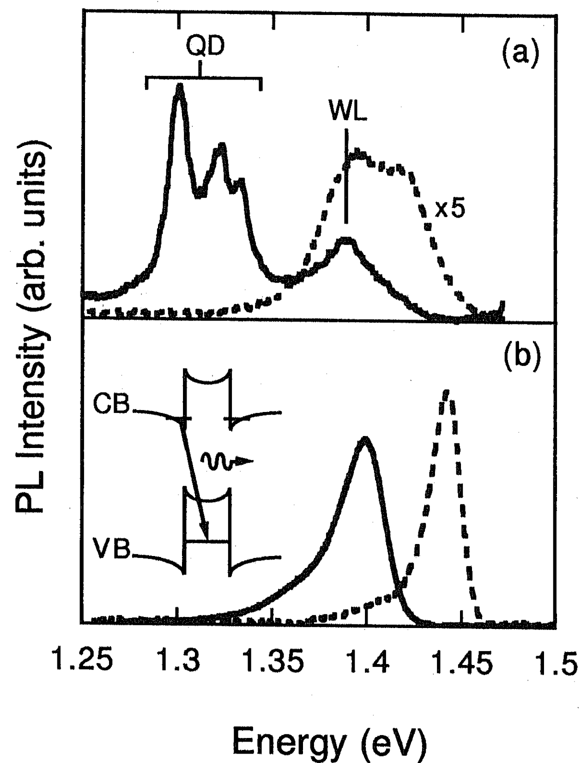

Fig. 3.3: PL spectra for the 2 ML quantum well (dashed line) and 2.5 ML quantum dots (solid line) samples obtained with excitation densities of ~6 W cm^{-2} at (a) 840 nm (~1.48 eV) and (b) 532 nm (~2.32 eV).

PL spectra for the 2 ML(QW) (dashed line) and 2.5 ML(QD) (solid line) samples obtained by excitation with 6 W/cm^2 at 840 nm (1.48 eV) and 6 W/cm^2 at 535nm (2.32 eV) are shown in Fig. 3.3 (a) and (b), respectively. PL measurements with a cooled PbS detector indicated no addition luminescence features between 0.5 and 1.25 eV other than those due to deep levels originating from the substrate. At an excitation energy of 1.48 eV, which is below the GaAs band-gap at these temperatures, absorption of the incident light should take place mainly in the GaSb layers giving a much smaller density of photo-excited carriers than in the case of excitation at 2.33 eV where all the incident light is absorbed. For the 2 ML(QW) sample, we

observe a feature which appears to consist of two peaks. Under higher photo-excited carrier densities the higher energy peak dominates (Fig. 3.3(b)). Under increasing injection power the peaks are observed to be blueshifted (~20 meV for the difference in excitation between Fig. 3.3(a) and Fig. 3.3(b)) which is consistent with a type-II band alignment[21]. In Fig. 3.3 (a) for the 2.5 ML(QD) sample we see features at 1.3-1.35 eV and a peak at 1.39 eV. The low energy features (1.3-1.35 eV) are attributed to the GaSb QDs, while the feature at 1.39 eV is attributed to the 2D wetting layer (WL). At higher photo-excited carrier densities (Fig. 3.3) the features at 1.3 eV are not clearly observed. We observe a tail to lower energies and a single peak dominating the spectra at 1.4 eV. This dominant peak appears to correspond to the WL .

Excited states

Figure3.4 shows the change in the PL spectra for the 2.5 ML(QD) sample as a function of excitation density for excitation at 840 nm (1.48 eV). At the lowest power density (0.95 W/cm^2) only one peak is clearly observed at 1.3 eV. As the power density is increased peaks to higher energy (20 and 35 meV) are observed. The intensity of these peaks increases until at the highest power obtainable, only one broad peak is resolved. We also note that the peak attributed to the wetting layer increases in intensity at a greater rate than the lower energy features attributed to the QDs. We consider that the feature at 1.3 eV corresponds to the ground state of the QDs, this luminescence having a full width at half maximum (FWHM) of 20 meV. The features at ~1.32 and ~1.335 eV are attributed to the excited states of the QD. The filling of the QD levels at these low excitation densities may be possible when we consider that the radiative lifetime of the type II QDs should be long.

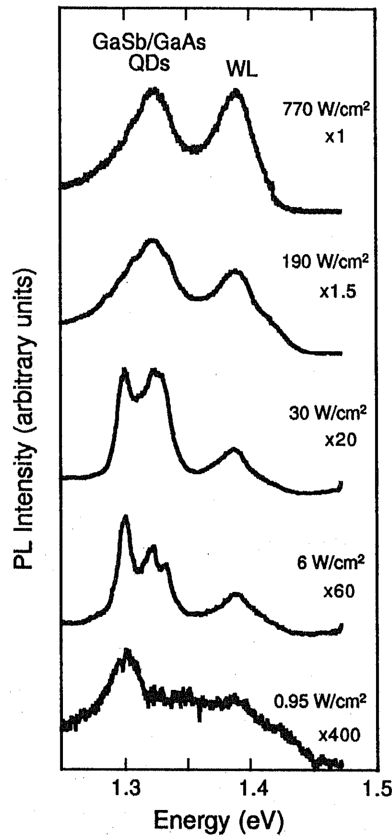

Fig. 3.4: PL spectra for the 2.5 ML quantum dot sample obtained at different power densities at 840 nm (1.48 eV).

In addition to this long lifetime, there is a low density (2×10^9 cm^{-2}) of dots for this sample. We therefore consider that the reason for the form of the PL spectra in Fig. 3.3 (b) is that at this relatively high density of photo-excited carriers, the dot levels are entirely saturated and the luminescence is dominated by the WL. Sun *et al.* have reported the measurement of the radiative lifetime of GaSb QD luminescence.[9] The PL spectra discussed were very similar to that for the 2.5 ML(QD) sample in Fig. 3.3 (b) which as we have discussed is dominated by luminescence from the WL. We consider that it is possible that the luminescence attributed to the QDs in that

case was actually related to the GaSb WL. We also note that Hatami *et al.* reported a blue-shift of QD related luminescence which was of a greater magnitude than that of the WL luminescence.[4] They attributed this shift to an increase in the Coulomb potential formed by the localized holes leading to an increase in the energy of the bound states of the electrons. We note that we observe an apparent blue-shift of the QD related luminescence and that this shift is greater than that of the WL luminescence. In this case, this apparent blueshift appears to be due mainly to the filling of the quantum dots.

3.5 Temperature Dependence

In order to discuss the PL stability and quality of the samples, the temperature dependence of the PL spectra were investigated. Figure 3.5 shows the temperature dependence of the PL spectra from the QDs and the WL. With increasing temperature, the PL from the QDs was more stable in intensity than that from the WL.

In order to identify the mechanism of PL quenching, the temperature dependence of the wavelength-integrated PL intensity is displayed in Fig. 3.6 (Arrhenius plot). These data can be fitted using the following equation :

$$I = Cexp(E_a/kT),$$

where C is a constant. We extract thermal activation energies E_a from the high temperature region. The QDs have a thermal activation energy of 130 meV. In comparison with the thermal activation energies of 46 meV [22] and ~120 meV [23] for InAs/GaAs QDs, our large activation energies for the GaSb/GaAs QDs are at-

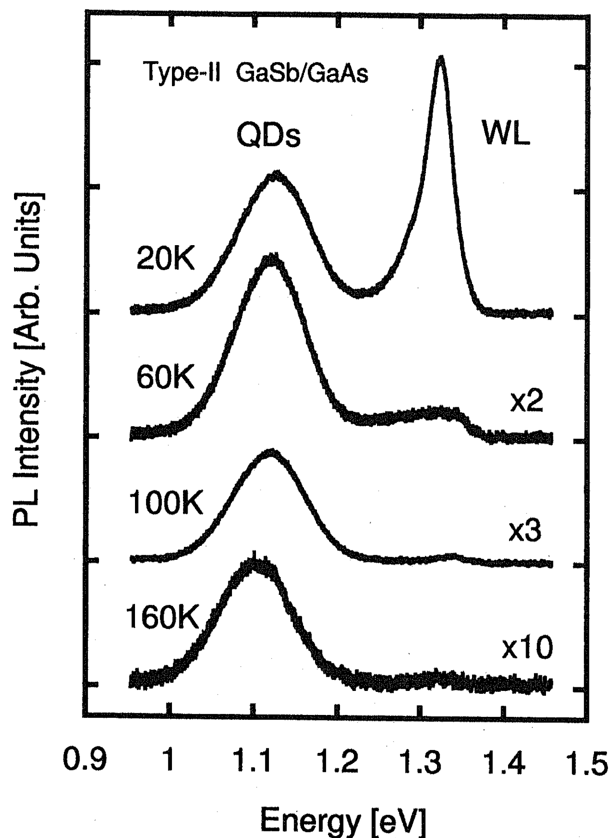

Fig. 3.5: Temperature dependence of PL spectra for the GaSb QDs. With increasing temperature, the intensity of PL from the QDs was more stable than that from the WL.

tributed to very strong localization of excitons in the QDs, even though the electrons and holes are spatially separated.

However, there are two slope in the WL case as shown in Fig. 3.6. These thermal activation energies in the wetting layer are extracted to be 67 meV and 18 meV in the higher and the lower temperature region, respectively. There are some possibility: (i) With increasing temperatures, carriers can be thermally activated. In this case, we suggest that the PL of the WL quenching is dominated by the recombination through

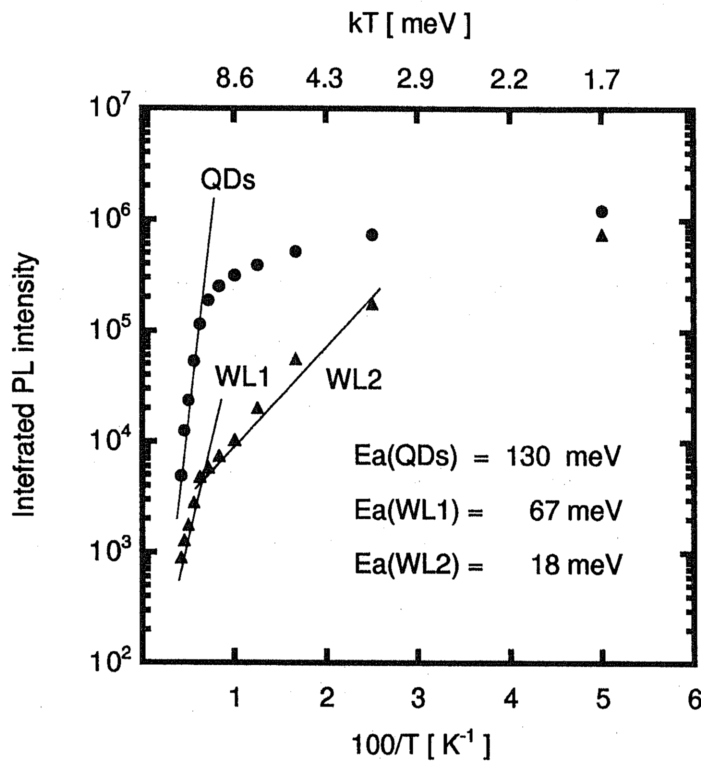

Fig. 3.6: Logarithm of the integrated PL intensity as a function of reciprocal temperature. Arrhenius plot shows the thermal activation energy of the GaSb QDs and the WL. It shows the thermal activation energy of the GaSb QDs to be 130 meV. There are two slopes for the WL case.

interface defects. One of the reason is considered that 5 minutes growth interruption was employed between the GaSb WL and the GaAs buffer. (ii) The observed thermal quenching of the PL is caused by the dissociation of excitons into the electron-hole pairs which can then escape from the WL via thermionic emission.[24, 25, 26] The energy (kT) of ~3 meV for the onset of the thermal quenching in the WL was extracted from 3.6. The thermal quenching energy in the QD is ~9 meV ,and is about three times larger than that in the WL. If it is corresponding to each exciton biding energies, it is mostly due to the difference of confinement dimension. The 3D confinement enhances the exciton binding energy.[27, 28, 29]

3.6 Photoluminescence Excitation Spectrum

Our assignment of the low energy peaks in Fig. 3.3(a) to the QDs is confirmed by Photoluminescence excitation (PLE) measurements obtained for the 2.5 ML(QD) sample, shown in Fig. 3.7. The lower part of this figure is a PL spectra taken with 6W cm^{-2} power density at an energy of 1.48 eV. The upper two traces correspond to two PLE spectra taken at different detection energies (marked by inverted triangles). There are a number of points which are noteworthy regarding these spectra. Firstly we note that there is a non-zero PLE signal at all excitation energies. This is consistent with the transition of a hole localized in the GaSb QD (and hence delocalized in k-space) to the GaAs conduction-band.

Furthermore, we observe an enhancement in the PLE spectra at an energy corresponding to the peak in PL attributed to the WL. This peak is most noticeable in the PLE spectra obtained by detecting at 1.298 eV. This is attributed to the relaxation of holes generated in the GaSb WL to the QD states. In both PLE spectra we also observe a feature at an energy ~25-27 meV higher than the detection energy.

If there is no energy dependence of the relaxation probability from the initially excited state to the ground state then it would be reasonable for the peaks in PLE due to the excited states to correspond to those observed in PL. However, there have been a number of reports concerning the observation that PLE spectra for InAs/GaAs QDs are dominated by peaks corresponding to the effects of carrier relaxation by the emission of LO phonons from excited states to the ground state of the QDs[31, 32]

In the present case of GaSb, the bulk LO phonon energy is 28.8 meV and a pre-

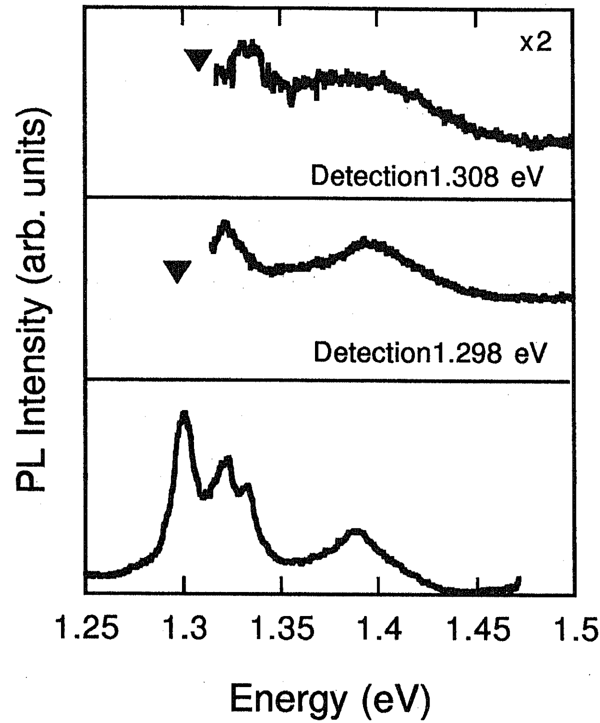

Fig. 3.7: PL spectra obtained by 6 W cm^{-2} excitation at 840 nm (1.48 eV) (bottom trace) and PLE spectra obtained at two different detection energies (triangles) for the 2.5 ML quantum dot sample.

vious report of Raman scattering measurements for GaSb QDs indicated a phonon energy of 29 meV[11]. As the width of the feature in PLE is too broad to correspond to a Raman related transition, and no Raman features corresponding to the GaAs matrix are observed, we attribute this feature to the excitation and enhanced relaxation of dots with ground states and excited states differing in energy by 1 GaSb LO phonon. The 2 LO phonon was not obtained.

We conclude that PLE measurements confirm our assignment of the QD related peaks and a feature 25-27 meV higher in energy than the PLE detection energy was discussed in terms of phonon relaxation.

3.7 Type-II Staggered Band Alignment

GaSb/GaAs band alignment with a hydrostatic strain

We discuss a type-II band alignment of GaSb/GaAs. The calculation is based on the model solid theory.[3] The strains in a pseudomorphic system can be determined by minimizing the macroscopic elastic energy. The lattice constant by symbol a; the subscript $||$ and $\perp$ are used to indicate quantities parallel or perpendicular to the plane of the interface. We can derive the strain tensors ϵ.

$$\epsilon_{||} = \frac{a_{||}}{a} - 1$$

$$\epsilon_{\perp} = -D\epsilon_{||}$$

It is for GaSb/GaAs(001) interface: first, consider the case of a thin GaSb overlayer on a GaAs substrate. This GaAs was fixed at $a_{||} = 0.565$ nm ; no strains are present in a GaAs. The lattice constants a of 0.608 nm was used for a GaSb. The constant (D) was used 0.910 for GaSb (001) [33]. If we choose a Cartesian coordinate system with x and y axes in the plane of the interface, and z axis perpendicular to interface [hence the notaion (001)], the components of the strain the strain tensor for GaSb are $\epsilon_{xx} = \epsilon_{yy} = -0.071, \epsilon_{zz} = 0.064$. All off-diagonal components are zero. This result in a volume charge $\Delta\Omega/\Omega = Tr(\epsilon) = (\epsilon_{xx} + \epsilon_{yy} + \epsilon_{zz})$ = -0.078. This volume charge determines the hydrostatic contribution of the strain, and will enter into the overall band lineups.

	Δ_0	$E_{v,av}$	a_v	E_g^{dir}	E_c^{dir}	a_c^{dir}	a^{dir}
GaAs	0.34	-6.92	1.16	1.52	-5.29	-7.17	-8.33
GaSb	0.82	-6.25	0.79	0.75	-5.23	-6.85	-7.64

Table 3-1 : Parameters of GaAs and GaSb for band lineups calculation. Spin-orbit splitting Δ_0 and energy gaps E_g were in Ref [30]. Values of $E_{v,av}$ (average of

three uppermost valence bands at Γ), $a_v = d(E_{v,av})/d(ln\Omega)$, $a_c = d(E_c/d(ln\Omega)$, and $a = d(E_c - E_{v,av})/(dln\Omega)$ were calculated with in the model-solid approach [3].

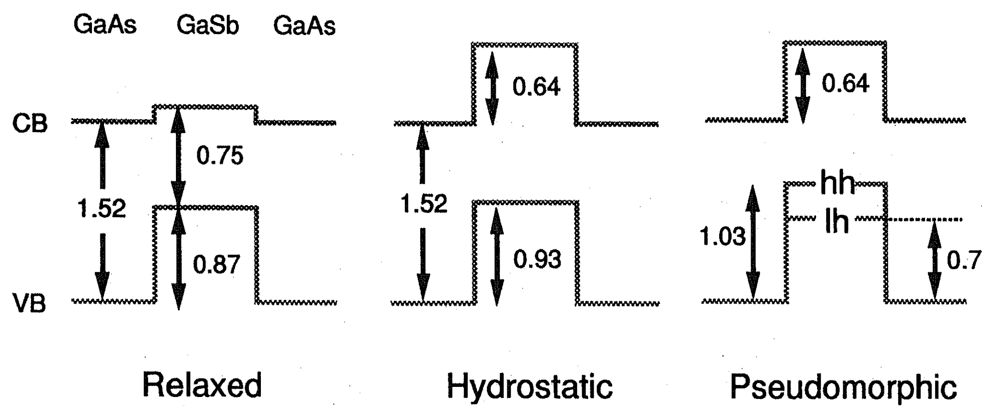

Fig. 3.8: Band lineups at a GaSb/GaAs interface. A relaxed unstrain, with a hydrostatic strain, and a pseudomorphic strain are shown. The discontinuity in the average valence bands, $\Delta E_{v,av}$, is obtained from model-solid theory. All energies are given by eV.

The positions of $E_{v,av}$ and E_c are affected by the volume change in the layers. The relation

$$E_{v,av} = E^0_{v,av} + a_v \frac{\Delta\Omega}{\Omega}$$

$$E_c = E^0_c + a_c \frac{\Delta\Omega}{\Omega}$$

expresses $E_{v,av}$ in terms of its value the unstrained material (i.e., the equilibrium-volume value from Table 3-1), the hydrostatic deformation potential for the valence

band a_v, and the fractional volume change $\Delta\Omega/\Omega = Tr(\epsilon) = (\epsilon_{xx} + \epsilon_{yy} + \epsilon_{zz})$. Then $\Delta E_{v,av}$ follows immediately. Conduction bands can be positioned in a similar manner, using the E_c values listed Table 3-1 and including the appropriate shifts due to strain. This leads to $\Delta E_{v,av} = 0.93$ eV (higher in GaSb) For the conduction bands, this also results in $\Delta E_c = 0.64$ eV. The lineups of the calculated GaSb/GaAs band alignment for different situations are shown in Fig. 3.8.

Charge potential

It was assumed that the hole was confined in the GaSb QD and the electron was confined around a GaAs. In effective mass treatment, the Hamiltonian for this spherical type-II GaSb/GaAs system is given by

$$H = -\frac{\hbar^2}{2m_e^*}\nabla_r^2 - \frac{\hbar^2}{2m_h^*}\nabla_r^2 + V_e(r_e) + V_h(r_h)$$

$$\nabla_r^2 = \frac{1}{r^2}\frac{\partial}{\partial r}r^2\frac{\partial}{\partial r}$$

$$V_e(r_e) = \begin{cases} -\frac{Ne^2}{4\pi\varepsilon r_e} - V_e & (r \geq a) \\ 0 & (r < a) \end{cases}$$

$$V_h(r_h) = \begin{cases} 0 & (r \geq a) \\ -V_h & (r < a), \end{cases}$$

where N is the number of holes. The last term of the Hamiltonian is the Coulomb attraction. In order to simplify, it was assumed that holes were almost entirely confined in the QD and were *not* affected from the electrons. Also, many body effects were neglected. The conduction band discontinuity V_e of 80 meV [34] was used. See chapter IV about the other deatail paremeters.

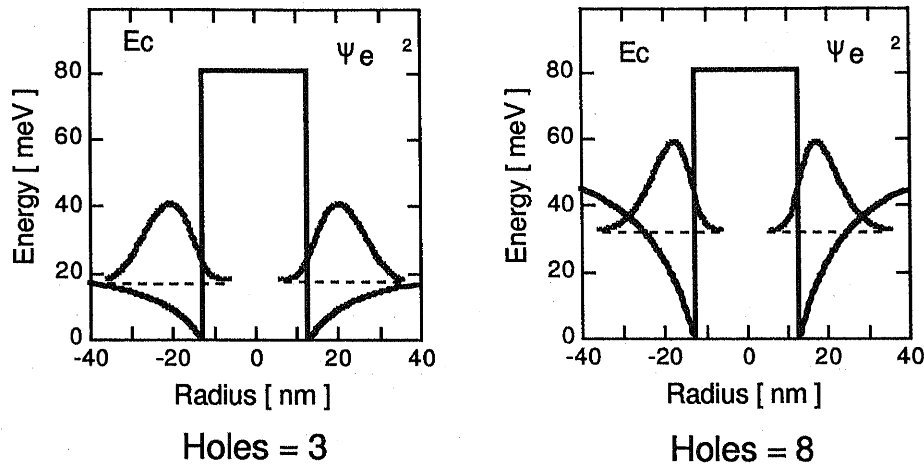

Fig. 3.9: Calculated electron wavefunctions in a spherical type-II quantum dot. The electrons localize around the dot due to the Coulomb potential. As a results, eigenvalues of electrons rise up with increasing charge (holes).

Figure 3.9 shows calculated electron wavefunctions in a spherical type-II quantum dot. The holes confined in the GaSb quantum dot. However, the electrons localize around the dot due to the Coulomb potential. As a results, eigenvalues of electrons rise up with increasing charge (holes). This calculated behavior of the blueshift with increasing charge is in good agreement with our experimental results. The blue shift with increasing the excitation power indicates type-II band alignment.

3.8 Summary

In chapter III, the features in photoluminescence (PL) measurements from the QDs were observed at ~1.1 eV, clearly separated from that of the wetting layer at ~1.3 eV. We observed a PL peak from the QDs clearly separated from that of

the WL. This result indicates that we have achieved successful control of As-Sb intermixing in GaSb/GaAs heterostructure despite the deposition of only a few ML of material.

With increasing excitation intensity, the peak from the QDs shifted towards higher energies, with a shift 6.5 times larger than that of the peak from the WL. It is due to increased charge density. Calculations based on the model performed in order to confirm it. The results are consistent with a type-II band alignment.

The optical properties of type II GaSb/GaAs QDs have been discussed. We have identified luminescence due to QDs by PL obtained at different excitation energies and densities. We have discussed how for these structures not only the spectral position of peaks, but also their relative intensities are critically dependent upon the density of photo-generated carriers.

In temperature dependence of photoluminescence measurements, we observed a thermal activation energy of 130 meV for the QDs luminescence indicating strong localization of excitons in the QDs.

PLE measurements have confirmed our assignment of the QD related peaks and a feature 25-27 meV higher in energy than the detection energy has been discussed in terms of phonon relaxation.

Bibliography

[1] Y. Arakawa, and H. Sakaki, Appl. Phys. Lett. **40** 932 (1982).

[2] S. Muto, Jpn. J. Appl. Phys. **34** L210 (1995).

[3] C. G. Van de Walle, Phys. Rev. B**39** 1871 (1989).

[4] F. Hatami, N. N. Ledentsov, M. Grundmann, J. Böhrer, F. Heinrichsdorff, M. Beer, D. Bimberg, S. S. Ruvimov, P. Werner, U. Goesele, J. Haydenreich, U. Richter, S. V. Ivanov, B. Ya. Meltser, P. S. Kop'ev, and Zh. I. Alferov, Appl. Phys. Lett.**67** 656 (1995).

[5] M. E. Rubin, H. -R. Blank, M. A. Chin, H. Kroemer, Appl. Phys. Lett.**70** 1590 (1997).

[6] E. R. Glaser, B. R. Bennett, B. V. Shanabrook and R. Magno, Appl. Phys. Lett.**68** 3614 (1996).

[7] R. A. Hogg, K. Suzuki, K. Tachibana, L. Finger, K. Hirakawa, and Y. Arakawa, Appl. Phys. Lett. **72** 2856 (1998).

[8] F. Hatami, M. Grundmann, N. N. Ledentsov, F. Heinrichsdorff, R. Heitz, J. Böhrer, D. Bimberg, S. S. Ruvimov, P. Werner, U. Goesele, J. Haydenreich, U. Richter, S. V. Ivanov, V. M. Ustinov, P. S. Kop'ev, and Zh. I. Alferov, Phys. Rev. B **57** 4635 (1998).

[9] C. -K. Sun, G. Wang, J. E. Bowers, B. Brar, H. -R. Blank, H. Kroemer, and M. H. Pilkuhn, Appl. Phys. Lett. **68** 1543 (1996).

[10] B. R. Bennett, R. Magno, and B. V. Shanabrook, Appl. Phys. Lett.**68** 505 (1996).

[11] B. R. Bennett, B. V. Shanabrook, and R. Magno, Appl. Phys. Lett.**68** 958 (1996).

[12] K. Suzuki, R. A. Hogg, K. Tachibana, and Y. Arakawa, Jpn. J. Appl. Phys. **37** L203 (1998).

[13] Chin-An Chang, R. Ludeke, L. L. Chang, and L. Esaki, Appl. Phys. Lett. **31** 759 (1977).

[14] M. Yano, M. Ashida, A. Kawaguchi, Y. Iwai, and M. Inoue, J. Vac. Sci. & Technol B**7** 199 (1989).

[15] N. N. Ledentsov, J. Böhrer, M. Beer,F. Heinrichsdorff, M. Grundmann, D. Bimberg, S. V. Ivanov, B. Ya. Meltser, S. V. Shaposhnikov, I. N. Yassievich, P. S. Kop'ev, and Zh. I. Alferov, Phys. Rev. **B52** 14058 (1995).

[16] J. M. Moison, F. Hpozay, F. Barthe, L. Leprince, E. Andre, and O. Vatel, Appl. Phys. Lett. **64**, 196, (1994).

[17] J.-Y. Marzin, J.M. Gerard, A. Izrael, D. Barrier, and G. Bastard, Phys. Rev. Lett. **73**, 716, (1994).

[18] S. Fafard, R. Leon, D. Leonard, J.L. Merz, and P.M. Petroff, Phys. Rev. **B50**, 8086, (1994).

[19] M. Grundmann, J. Christen, N.N. Ledentsov, J. Boehrer, D. Bimberg, S.S. Ruvimov, P. Werner, U. Richter, U. Goesele, J. Heydenreich, Y.M. Ustinov, A.Yu. Egorov, A.E. Zhukov, P.S. Kop'ev, and Zh.I. Alferov, Phys. Rev. Lett. **74**, 4043, (1995).

[20] U.E.H. Laheld, F.B. Pederson, and P.C. Hemmer, Phys. Rev. B **52**, 2697, (1995).

[21] M.S. Bressler, O.B. Gusev, M.P. Mikhailova, V.V. Sherstnev, Yu. P. Yakovlev, and I.N. Yassievich, Sov. Phys. Semicond. **25**, 181, (1991).

[22] D. I. Lubyshev, P. P.Gonzá lez-Borrero, E. Marega, Jr., E. Petitprez, N. La Scala, Jr., and P. Basmaji, Appl. Phys. Lett.**68** 205 (1996).

[23] Z. Y. Xu, Z. D. Lu, X .P.Yang, Z. L. Yuan, B. Z. Zheng, J. Z. Xu, W. K. Ge, Y. Wang, and L. L. Chang, Phys. Rev. B**54** 11528 (1996).

[24] G. Bacher, C. Hartmann, H. Schweizer, T.Held, G. Mahler, and H. Nickel, Phys. Rev. B**47** 9594 (1993).

[25] J. D. Lambkin, D. J. Dunstan, K. P. Homewood, L. K. Howard, and M. T. Emeny, Appl. Phys. Lett.**57** 1986 (1990).

[26] M. Venning, D. J. Dunstan, and K. P. Homewood, Phys. Rev. B**48** 2412 (1993).

[27] G. W. Bryant, Phys. Rev. B**37** 8763 (1988).

[28] S. LeGoff and B. Stebe, Phys. Rev. B**47** 1383 (1993).

[29] Y. Kayanuma, Phys. Rev. B**44** 13085 (1991).

[30] *Landolt-Börnstein, Numerical Data and Functional Relationship in Science and Techology* (Springer, New York, 1982), Group III, Vol.17a-b.

[31] M.J. Steer, D.J. Mowbray, W.R. Tribe, M.S. Skolnick, M.D. Sturge, M. Hopkinson, A.G. Cullis, C.R. Whitehouse, and R. Murray, Phys. Rev. B **54**, 17738, (1996).

[32] R. Heitz M. Grundmann, N.N. Ledentsov, L. Eckey, M. Veit, D. Bimberg, A.Yu. Egorov, P.S. Kop'ev, and Zh.I. Alferov, Appl. Phys. Lett. **68**, 361, (1996).

[33] W. F. Boyle and R. J. Sladek, Phys. Rev. B **11**, 1587 (1975).

[34] M. E. Rubin, H. -R. Blank, M. A. Chin, H. Kroemer, Appl. Phys. Lett. **70** 1590 (1997).

Chapter 4

Time-resolved Photoluminescence of Type-II GaSb/GaAs Quantum Dots

4.1 Introduction

The GaSb/GaAs quantum dot (QD) should exhibit a type-II band-alignment. In this case, holes are localized within the GaSb QD, while due to Coulomb attraction the electrons form a shell around the QD. Therefore, the radiative life times for the type-II QDs are longer than those for a type-I QDs (e.g. InAs/GaAs).[1, 2] The possible realization of a frequency-selective optical memory using QDs has been proposed [3] which relies upon hole burning. Type-II QDs may be more useful than type I QDs for such optical memories. GaSb/GaAs heterostructures have attracted a great deal of interest due to the possibility of novel device Also, the QDs therefore allow semiconductor artificial atoms to be realized. Compared with conventional type-I QDs such as InGaAs/GaAs QDs, relatively few studies of carrier dynamics in type-II QDs have been reported [1, 2]. Therefore, further detailed investigation of carrier dynamics in type-II QDs is required.

In this chapter, we report time-resolved photoluminescence measurements of

type-II GaSb/GaAs self-assembled quantum dots (QDs). The dynamic behavior of the QDs and the wetting layer are systematically investigated. In particular, excitation power dependence of time-resolved photoluminescence measurements reveals the interesting behavior in the type-II band alignment. In addition, the conduction band discontinuity of the QDs is discussed. The results of calculations are compared with experiments. It allows to extract the conduction band offset.

4.2 Time-resolved Photoluminescence Setup

We have grown GaSb/GaAs self-assembled QDs by molecular beam epitaxy (MBE) [4, 5]. Here the quantum dot (QD) samples were grown by MBE (VG Semicon V80H Mark III) on GaAs (001) substrates. The surfaces were characterized by atomic force microscopy (AFM). The QDs had a lateral diameter (~25 nm), a height (~6 nm), and a density (1.2×10^{10} cm^{-2}) at the deposition of 3.1 ML GaSb on GaAs. Since our measurements are limited by the tip shape of AFM, the actual lateral diameters are smaller than the measured ones. Another sample was capped by a 50 nm GaAs layer for optical measurements. The details of the growth technique have been described in chapter II.

Ti:sapphire lasers with a pulse picker

We consider how to measure the time-resolved photoluminescence of type-II quantum dots. First, the quantum dots have long decay due to spatially exciton. Therefore, the reputation of pulse lasers have to be enough much. Conventional Ti:sapphire lasers have the reputation rate of 72 MHz. It is too high frequency for the type-II QDs. The reputation of 78 MHz is corresponding to ~13 ns. Therefore, the pulse of Ti:sapphire lasers is reduced 4.8 MHz with a plus picker.

Time-correlated single photon counting (TCPC) system

The quantum dots have emission at 1.1 eV. Various technique can be utilized to perform time-resolved photoluminescence measurements. Table 4-1 shows a comparison of time-resolved photoluminescence measurements techniques. It is difficult to detect a signal with a streak camera system. Also it is not so excellent to characterize long decay with a streak camera system. However, time-correlated single photon counting (TCPC) system has an advantage of a large dynamic range. Also, the detection of signals depend on detectors. Thus, high sensitive detector at 1.1 eV is available. However, the time resolution is limited by detection electronics and the response of detector. In this case, it is not required so high resolution. Consequencely, time-correlated photon counting techniques were employed to investigate lifetimes

	Time-correlated photon counting	Streak camera
Sensitivity	very high	high
Dynamic range	very high	normal
Time resolution	150-600 ps	1-10 ps

Table 4-1 : A comparison of time-resolved photoluminescence measurements techniques. Time-correlated photon counting techniques were employed to investigate lifetimes of type-II GaSb/GaAs quantum dots.

Experimental setup

Figure 4.1 show the experimental setup. The time-resolved photoluminescence (PL) measurements were performed by a time-correlated photon counting (TCPC) technique. The sample was cooled to low temperature (20K) in a closed-cycle helium cryostat, in order to investigate the intrinsic radiative lifetimes of the QDs. The laser system consisted of a mode-locked Ti:sapphire laser (Coherent Mira 900) at 780 nm and a pulse picker with 4.8 MHz repetition rate. The PL from the QDs and the wetting layer (WL) was selected by using band-pass filters of 1100 nm $\pm$ 5 nm ($\sim$1.1 eV) and 950 nm $\pm$ 5 nm ($\sim$1.3 eV), respectively. The PL was detected by a liquid nitrogen cooled InGaAsP/InP photo multiplier tube (Hamamatsu photonics R5509-41) which was sensitive up to 1.4 μm. The TCPC technique was carried out with a time amplitude converter (TAC) by Hamamatsu photonics. This system has a time resolution of $\sim$600 ps.

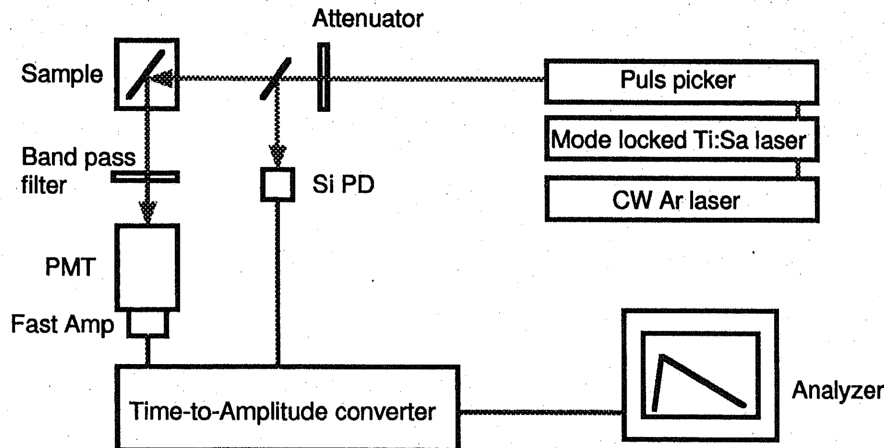

Fig. 4.1: An experimental setup of the time-resolved photoluminescence measurements by a time-correlated photon counting (TCPC) technique.

4.3 Time-resolved Photoluminescence

Exciton recombination in quantum dots

The radiative decay rate (Γ) of excitons is expressed by:

$$\Gamma = \Gamma_0 \left|\langle\psi_{electron}|\psi_{hole}\rangle\right|^2 \left(\frac{L}{a_B}\right)^n,$$

where n is 3 for quantum dot structures and a_B is the Bohr radius. The first term, Γ_0, is the oscillator strength per unit volume. The Γ_0 is an intrinsic property of semiconductor material. It is directly proportional to the bandgap energy of the semiconductor material. This factor contributes significantly to the decreases of the exciton lifetimes with the transition energy. The second term, $|\langle\psi_{electron}|\psi_{hole}\rangle|^2$, is the square of the wavefunction overlap between the electron and the hole. The value is affected by the quantum dot dimension, the confinement potential, and the effective masses of the electron and the hole. Larger wavefunction overlap is obtained with a higher potential barrier and a smaller confinement dimension. However, for light mass particle, the effect of a small confinement dimension will push the wavefunction into the barrier, reducing the wavefunction overlap. The wavefunction overlap does not depend strongly on the material system. The effect is mainly observed through the variation in the lateral dot size.

Type-II GaSb/GaAs quantum dots

Figure 4.2 inset shows PL spectrum from the GaSb QDs and the WL. Excitation intensities were (i) 0.56 W/cm^2, (ii) 2.2 W/cm^2, and (iii) 5.6W/cm^2, respectively. Here the excitation was chopped and the signal recovered by standard lock-in techniques. In particular, the separate PL features from the QDs (~1.1 eV) and the WL (~1.3 eV) were clearly observed. The PL from the QDs and the WL have full width

at half-maximum (FWHM) of ~100 meV and ~40 meV, respectively. We are able to discuss these intrinsic carrier dynamics using coherent GaSb/GaAs QDs (~25 nm). These peaks were shifted towards higher energies with increasing excitation intensity. Both the formation of the dipole layer and the QDs state filling contributed to the blueshifts of the PL peaks. This is evidence of type-II band alignment and has been reported [1, 2, 5, 6].

Figure 4.2 (a) and (b) show the excitation intensity dependence of the time-resolved PL measurements of the QDs and the WL at 20 K. Excitation intensities were (i) 0.56 W/cm^2, (ii) 2.2 W/cm^2, and (iii) 5.6W/cm^2, respectively. The measured PL data were normalized with the peaks. The decay is not a single exponential. The non single exponential decay was discussed by C.-K.Sun *et al.* [1]. In order to extract time constants from our data, we fitted an exponential function to the initial decay. The QDs in Fig. 4.2 (a) exhibited a decay time of τ_{QDs} ~23 ns at the lowest excitation power of 0.56 W/cm^2. These results are considerably longer than lifetimes ($\tau_{InGaAsQDs} = 1$ ns) of a typical type-I band alignment in InGaAs/GaAs QDs [8, 9]. A few similar results of time-resolved PL measurements for GaSb/GaAs QDs have been reported. The observed lifetimes of the initial decay were 9 ns [1] and 5 ns [2].

The WL exhibited the initial decay of τ_{WL} ~17 ns at 0.56 W/cm^2. The initial decay of the WL was faster than that of the QDs. The decay times for the WL and QDs depend on a number of parameters, making a quantitative analysis difficult. We observed a relatively strong WL luminescence peak even at low pump powers, where the QDs state filling can be neglected (average hole occupancy $\leq$1 per QD). Also decay of the WL luminescence puts an upper limit on relaxation rate of carriers to QDs of 17 ns at 0.56 W/cm^{-2}. It is therefore clear that carrier scattering from the WL to the QD is slower than in type-I InAs/GaAs QDs. The rise time of the QD PL is limited by the temporal response of the measurement ~ 600 ps. Carriers

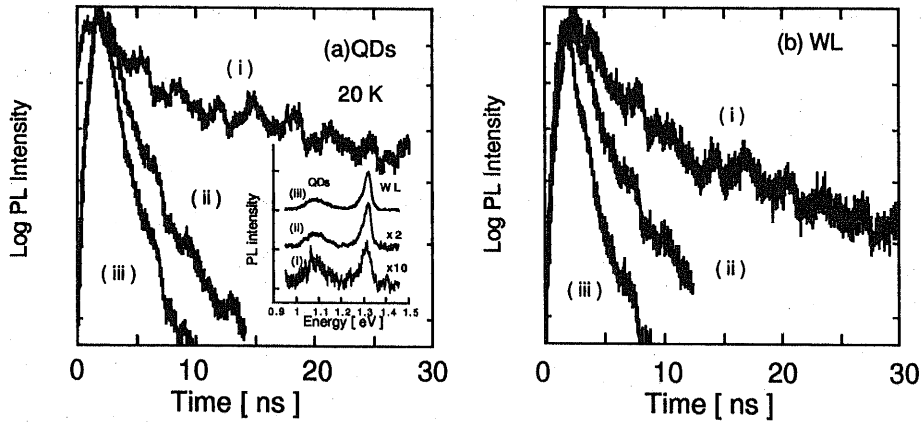

Fig. 4.2: Time-resolved PL of type-II GaSb/GaAs (a) the QDs at ~1.1 eV and (b) the WL at ~1.3 eV Excitation intensities were (i) 0.56 W/cm^2, (ii) 2.2 W/cm^2, and (iii) 5.6W/cm^2, respectively. Inset shows PL spectrum from the QDs and the WL.

are therefore relaxing to the QDs on a time scale shorter than this. This suggests that carriers are captured quickly by the QDs directly from the bulk, bypassing the WL.

In this result, we cannot explain it enough, so that it is impossible to claim the difference of the charge. However, the lifetimes of the QDs were always longer than that of the WL. One potential argument for it would be a phonon bottleneck effect, where the carrier scattering rate from the barrier into the QDs is reduced. We also agree with their explanation.

4.4 Excitation Intensity Dependence

The radiative lifetimes strongly depended on excitation intensity. Figure 4.3 shows the lifetimes fitted with the initial decay as a function of excitation power densities in the type-II GaSb/GaAs QDs and WL. Figure 4.3 inset shows a schematic diagram of the structure. The radiative lifetimes were shortened with increasing excitation intensity.

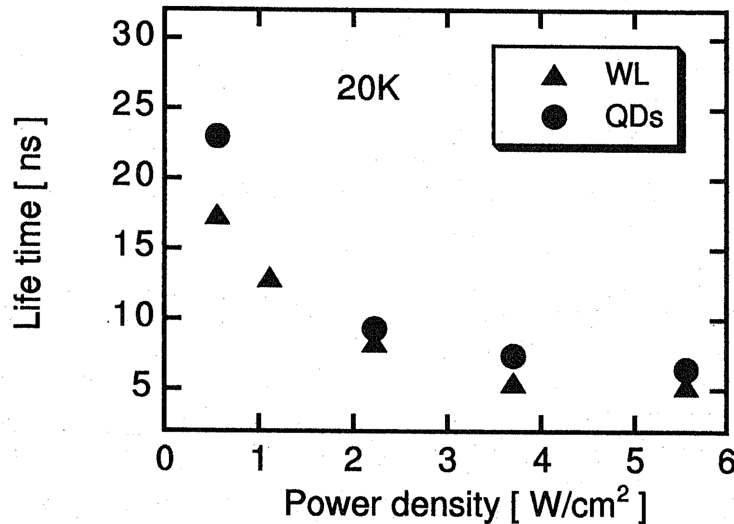

Fig. 4.3: The radiative lifetimes fitted with the initial decay as a function of excitation power densities for the type-II GaSb/GaAs QDs and WL. Inset shows a schematic diagram of the structure.

There are two key observations : (i) the radiative lifetimes are drastically shortened with increasing excitation intensity, and (ii) the radiative lifetimes of the QDs are always longer than those of the WL. The evidence of (i) is attributed to Coulomb attraction in spatially indirect excitons in a staggered (type-II) band alignment. In

this case, holes are localized within the QDs, while due to the Coulomb attraction the electrons form a shell around the QDs. The band bending of the conduction band increases with increasing hole densities. This means that the oscillator strength is enhanced with increasing excitation intensity. Besides, similar results have supported a staggered band lineup and space charge included band-bending model [1, 2, 5, 6].

4.5 Conduction Band Offset

Band discontinuities are key points in heterostructures. The conduction band discontinuity of the QDs is discussed. The model solid theory [10] predicts a giant conduction band discontinuity of 640 meV in the GaSb/GaAs heterostructure when strain effects are considered. However, M. E. Rubin *et al.* have reported a conduction band offset of 80 meV [11] in the GaSb/GaAs QDs, where ballistic electron emission microscopy was used to map individual QDs. We carried out a simple calculation, in order to investigate the offset, The GaSb/GaAs heterostructure should exhibit the type-II band alignment as shown in Fig. 4.4 inset. In addition, the long decay time is attributed to the slow radiative recombination between Γ state holes in the GaSb QDs and Γ state electrons in the GaAs [1].

Therefore, an electron-hole overlap squared in a simplified model of a spherical QD with a radius (a) was numerically calculated in spherical coordinates. It was assumed that the hole was confined in the GaSb QD and the electron was confined around a GaAs. In effective mass treatment, the Hamiltonian for this spherical type-II GaSb/GaAs system is given by

$$H = -\frac{\hbar^2}{2m_e^*}\nabla_r^2 - \frac{\hbar^2}{2m_h^*}\nabla_r^2 + V_e(r_e) + V_h(r_h) + V_{Coulmb}(r_e)$$

$$\nabla_r^2 = \frac{1}{r^2}\frac{\partial}{\partial r}r^2\frac{\partial}{\partial r}$$

$$V_{Coulmb}(r_e) = \begin{cases} -\frac{Ne^2}{4\pi\varepsilon r_e} & (r \geq a) \\ 0 & (r < a), \end{cases}$$

where N is the number of holes. The last term of the Hamiltonian is the Coulomb attraction. In order to simplify, it was assumed that holes were almost entirely confined in the QD and were *not* affected from the electrons. Also, many body effects were neglected. The following parameters were employed. The effective masses of the electron and the hole are $m_e^* = 0.067m_0$ and $m_h^* = 0.45m_0$ for a GaAs, while $m_e^* = 0.049m_0$ and $m_h^* = 0.33m_0$ for a GaSb, respectively. The mixing of the light and heavy holes was neglected. Holes are confined in finite potential of $V_h = 0$ for $r \geq a$, and $V_h = -0.9$ eV [10] for $r < a$. On the other hand, electrons are confined in finite potential of $V_e = -const$ for $r \geq a$, and $V_e = 0$ for $r < a$. The dominant factor of the oscillator strength is an electron envelope function, since the effective mass of electrons is smaller than that of holes. The dielectric constants ε_r, in $\varepsilon = \varepsilon_r\varepsilon_0$, were assumed to be an average value between $\varepsilon_{GaAs} = 13.31$ and $\varepsilon_{GaSb} = 15.69$. Here the radius ($a$) of the QDs was 5 nm. Then an electron-hole overlap squared ,$| \langle\psi_e \mid \psi_h\rangle |^2$, was calculated with varied conduction band offset of V_e as shown in Fig. 4.4. The overlap squared strongly depended on a conduction band discontinuity V_e rather than the number of holes.

This separation reduces the electron-hole spatial overlap. The radiative recombination lifetimes τ_r are given by

$$\tau_r = \frac{\tau_0}{|M_{cv}|^2}$$

in the one-particle picture, where $|M_{cv}|^2$ is the overlap integral of the electron and hole wave functions [7], and τ_0 are the lifetimes under flat bind condition.

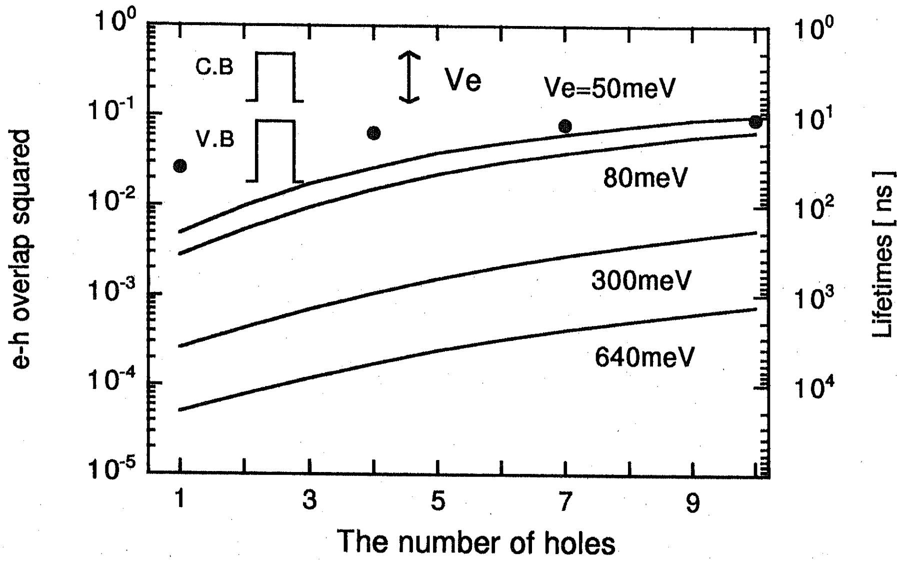

Fig. 4.4: The calculated electron-hole overlap squared, $\mid \langle \psi_e \mid \psi_h \rangle \mid^2$, as a function of the number of holes N at various values of the conduction band discontinuity V_e. The experiment results were plotted by dots with the number of holes, N, deduced from the excitation intensity. A conduction band offset of ~50 meV was extracted. Inset shows a schematic diagram of the GaSb/GaAs type-II band alignment in real space.

These calculations were compared with the experimental ones. Since the type-I QDs have electron-hole overlap of almost 100 %, an assumption,$\mid \langle \psi_e \mid \psi_h \rangle \mid^2 = 1$ at $\tau = 1$ ns, was used. This is based on the observed lifetimes of type-I InGaAs/GaAs QDs [8, 9]. For excitation a pulse laser with the reputation rate of 4.8 MHz was used, which means 120 nJ/cm^2 at 0.56 W/cm^2. The corresponding carrier density for the QDs is estimated $\sim 1 \times 10^{10}$ cm^{-2}. The sample had a QD density of 1.2 $\times$ 10^{10} cm^{-2}. Therefore, the excitation power density of 0.56 W/cm^2 is assumed to correspond to N=1. The electron-hole overlap squared increased with decreasing the offset as shown in Fig. 4.4. The band discontinuity of ~50 meV was extracted. This value is in good agreement with Rubin's experiments of 80 meV [11]. However, it is in strong disagreement with the giant offset which was theoretically predicted

to be 640 meV [10].

4.6 Summary

In chapter IV, we have performed time-resolved PL measurements on type-II GaSb/GaAs self-assembled QDs which were grown by MBE. The dynamic behavior of the QDs and the WL was systematically investigated. The radiative lifetimes (∼23 ns) in the QDs were considerably longer than those in type-I QDs. The initial decay was shortened with increasing excitation intensity. This is attributed to spatially indirect excitons in a staggered (type-II) band alignment. In addition, a conduction band discontinuity of the QDs was discussed. The offset of ∼50 meV was extracted.

Bibliography

[1] C. -K. Sun, G. Wang, J. E. Bowers, B. Brar, H. -R. Blank, H. Kroemer, and M. H. Pilkuhn, Appl. Phys. Lett. **68** 1543 (1996).

[2] F. Hatami, M. Grundmann, N. N. Ledentsov, F. Heinrichsdorff, R. Heitz, J. Böhrer, D. Bimberg, S. S. Ruvimov, P. Werner, U. Goesele, J. Haydenreich, U. Richter, S. V. Ivanov, V. M. Ustinov, P. S. Kop'ev, and Zh. I. Alferov, Phys. Rev. B **57** 4635 (1998).

[3] S. Muto, Jpn. J. Appl. Phys. **34** L210 (1995).

[4] K. Suzuki, R. A. Hogg, K. Tachibana, and Y. Arakawa, Jpn. J. Appl. Phys.**37** L203 (1998).

[5] R. A. Hogg, K. Suzuki, K. Tachibana, L. Finger, K. Hirakawa, and Y. Arakawa, Appl. Phys. Lett.**72** 2856 (1998).

[6] F. Hatami, N. N. Ledentsov, M. Grundmann, J. Böhrer, F. Heinrichsdorff, M. Beer, D. Bimberg, S. S. Ruvimov, P. Werner, U. Goesele, J. Haydenreich, U. Richter, S. V. Ivanov, B. Ya. Meltser, P. S. Kop'ev, and Zh. I. Alferov, Appl. Phys. Lett.**67** 656 (1995).

[7] G. Bastard, E. E. Mendez, L. L. Chang, and L. Esaki, Phys. Rev. B**28** 3241 (1983).

[8] G. Wang, S. Fafard, D. Leonard, J. E. Bowers, J. L. Merz, P. M. Petroff, Appl. Phys. Lett. **64** 2815 (1994).

[9] K. Mukai, N. Ohtsuka, H. Shoji, and M. Sugawara, Phys. Rev. B **54** 5243 (1996).

[10] G. C. Walle, Phys. Rev. B**39** 1871 (1989).

[11] M. E. Rubin, H. -R. Blank, M. A. Chin, H. Kroemer, Appl. Phys. Lett. **70** 1590 (1997).

Chapter 5

Magneto-photoluminescence of Type-II GaSb/GaAs Quantum Dots

5.1 Introduction

Recent advances in fabrication techniques have made possible nanostructures, so that it allows a study on strong zero-dimensional (0D) quantum confinement effects with δ-function-like density of states.[1, 2, 3] A lots of groups have performed photoluminescence measurements of quantum dots in magnetic fields.[4, 5, 6, 7] However, a magneto-photoluminescence study on quantum dots of type-II band alignment has not yet been reported. In this case, holes are localized within the GaSb quantum dot (QD), while due to Coulomb attraction the electrons form a shell around the QD. Therefore, magneto-excitons in type-II quantum dots is expected to be quiet different behavior compared to typical type-I quantum dots.

In this chapter, a systematic photoluminescence study on type-II GaSb/GaAs quantum dots in magnetic fields up to B = 8 T are presented. The diamagnetic shifts and the integrated intensity in magnetic fields are obtained. The effective size of excitons can be evaluated by studying the energy shift of photoluminescence in

magnetic fields. Compared with type-I quantum dots, the exciton behavior of type-II quantum dots are discussed. In addition, the exciton binding energy of type-II quantum dots are theoretically calculated by a variational method.

5.2 Photoluminescence in Magnetic Fields

Sample and experiment

GaSb/GaAs quantum dot structures were grown by molecular beam epitaxy, under conditions optimized for the self-assembled quantum dots.[8] The GaSb self-assembled quantum dots were grown on a GaAs and capped by 50 nm GaAs. The quantum dots have a diameter 25 nm, height 6 nm, and density 10^{10} cm^{-2} observed by atomic force microscopy. The sample was studied in magnetic fields up to 8 T at 4.2 K. The quantum dots were investigated with the magnetic field applied perpendicular (B⊥) to the wetting layer plane. Faraday (B||Z) geometry light propagating along the Z growth direction was used in the present photoluminescence measurements. Figure 5.1 shows a schematic drawing of type-II excitons in magnetic fields.

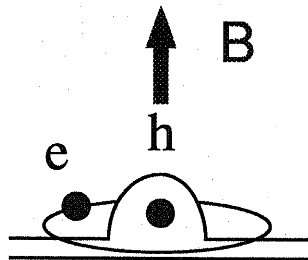

Fig. 5.1: A schematic drawing of type-II excitons in magnetic fields.

Photoluminescence in magnetic fields

Figure 5.2 shows magneto-optical photoluminescence spectra of the ground state in type-II GaSb/GaAs quantum dots. In our experiments, magnetic fields of 0 - 8 T were applied. Diamagnetic shifts under higher magnetic fields are proportional to the square of the magnetic field. As magnetic fields perpendicular to the quantum dots was increased, the exciton resonance showed diamagnetic shifts and its integrated intensity increased. The diamagnetic shift about ~0.9 meV up to 8 T were observed in the measured field region in the quantum dots.

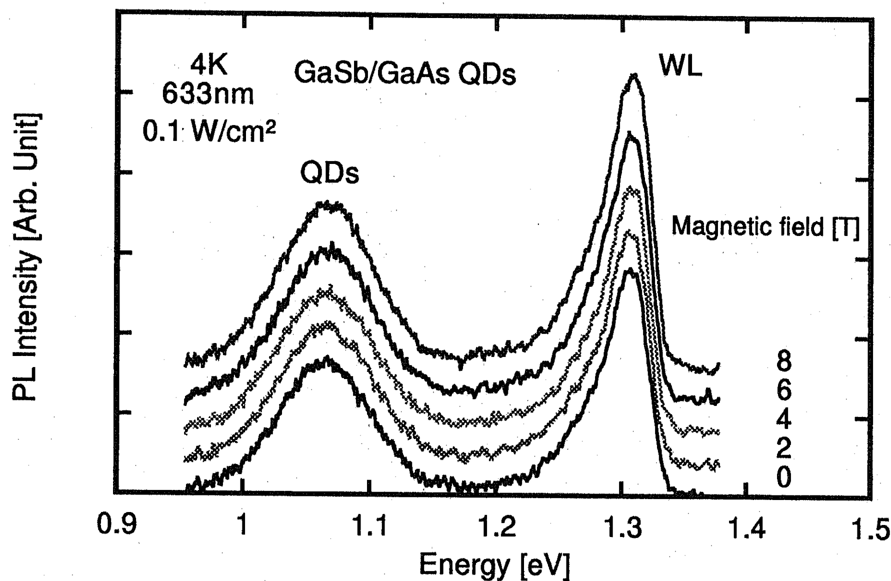

Fig. 5.2: Photoluminescence spectra of type-II GaSb/GaAs quantum dots in magnetic fields at 4 K. The magnetic field is perpendicular to the quantum dots.

5.3 Diamagnetic Shifts

In this type-II band alignment, we expect that electrons around the quantum dots are dominant factors in diamagnetic shifts. Contrarily, holes are strongly localized inside the quantum dots. In this case, holes are localized within the GaSb QDs, while due to Coulomb attraction the electrons form a shell around the QDs in a GaAs.

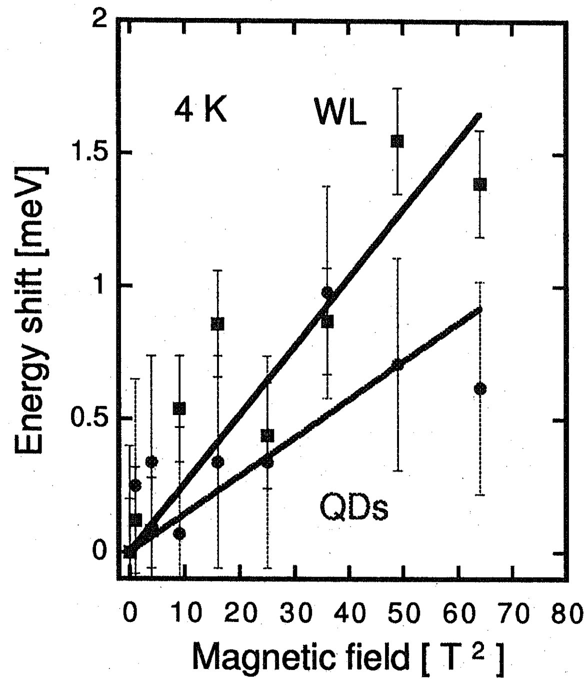

Fig. 5.3: Diamagnetic shifts in magnetic fields in the type-II GaSb/GaAs.

Figure 5.3 indicates that the PL peak exhibits a diamagnetic shift. As shown in Fig. 5.3, the average value of the photoluminescence energy can be fitted well by a parabolic dependence of magnetic fields, which gives a β of ~14 μ eV T^{-2} for

the GaSb/GaAs quantum dot. Also, the $\beta = \sim 25\ \mu$ eV T^{-2} was obtained for the GaSb/GaAs wetting layer. The difference is caused by dimensions of confinement.

The diamagnetic shift was expressed as $\Delta E = \beta B^2$ with diamagnetic coefficient β being equal to

$$\beta = \frac{e^2 \langle r^2 \rangle}{8\mu},$$

where

$$\langle \Psi \mid r^2 \mid \Psi \rangle \equiv \langle r^2 \rangle$$

characterizes the exciton localization. The exciton reduced mass is taken $\mu^{-1} = (m_e^{-1} + m_h^{-1}) = 0.057 m_0$ is used. Therefore, we can calculate effective areas $2 \langle r^2 \rangle$ using the diamagnetic coefficients β from our experimental data. As a results, we then obtain $2\sqrt{\langle r_{QDs}^2 \rangle} = 12$ nm for the in-plain spatial extent of the wave function around GaSb/GaAs quantum dots as shown in Table 5.1. Also, $2\sqrt{\langle x_{WL}^2 \rangle} = 16$ nm for the wetting layer was obtained.

	β (μeV T^{-2})	$2\sqrt{\langle r^2 \rangle}$ (nm)
Quantum dots	14	12
The wetting layer	25	16

Table 5.1 : Observed diamagnetic shifts and effective exciton diameters of the type-II GaSb/GaAs.

We compare with typical type-I quantum dots. The spatial extent of the carrier wave function in a type-I quantum dot have 10 nm observed by P.D.Wang *et al.*[4] and 6 nm by I.E.Istkevich *et al.*[5]. These values are two times smaller than that, $2\sqrt{\langle r_{QDs}^2 \rangle} = 12$ nm, in the type-II GaSb/GaAs. We interpret that these effects are

due to type-II band alignment. However, the $2\sqrt{\langle r^2_{QDs}\rangle}$ is not consistent with the base diameter (~25 nm) observed by atomic force microscopy. The confinement of the height (~6 nm) is dominant rather than the base diameter. We suppose that the in-plane confined potential mostly located on top region in a pyramidal shape dot.

In an ideal 2D quantum well, the in-plane exciton radius can be expressed as

$$\sqrt{r_{2D}} = \sqrt{\frac{3}{8}}\, a_B$$

with 3D exciton Bohr radius

$$a_B = \frac{\varepsilon\hbar^2}{\mu e^2}.$$

Hence, the dielectric constants ε_r, in $\varepsilon = \varepsilon_r\varepsilon_0$, were assumed to be an average value $\varepsilon_{ave} = 14.5$ between $\varepsilon_{GaAs} = 13.31$ and $\varepsilon_{GaSb} = 15.69$. The exciton reduced mass is taken $\mu^{-1} = 0.057m_0$ was used. We obtain $2a_B = 27$ nm and $2\sqrt{r_{2D}} = 16$ nm. Table 5.2 shows calculated 3D and 2D limit Bohr diameters in a GaSb/GaAs. This analysis indicates that zero-dimensional quantum confinement squeezes the exciton wavefunction beyond the 2D limit ($\sqrt{r_{2D}}$). Therefore, the lateral quantum confinement in the GaSb/GaAs quantum dots was confirmed. In addition, the in-plane exciton diameter of the wetting layer (2 ML) is in good agreement with the theoretical 2D limit value.

$2a_B$ (nm)	$2\sqrt{r_{2D}}$(nm)
27	16

Table 5.2 : Calculated 3D and 2D limit Bohr diameters in a GaSb/GaAs.

5.4 Oscillator Strength

The influence of magnetic fields on exciton wave function is determined by the ratio of cyclotron energy of electrons and holes, $\hbar\omega_c = e\hbar B/\mu$, and the exciton binding energy E_b, i.e., $\xi = \hbar\omega_c/2E_b$, where $-e$ is the electron charge, $\hbar$ is Planck's constant divided by $2pi$, B is the magnetic fields strength, and μ is the reduced effective mass. In low field limit of $\xi << 1$, the magnetic fields only perturb exciton states, hardly their wave function. On the other hands, in the high field limit of $\xi >> 1$, where electrons and holes are under cyclotron motion and perturbation from Coulomb interaction generates bound states belonging to Landau levels.

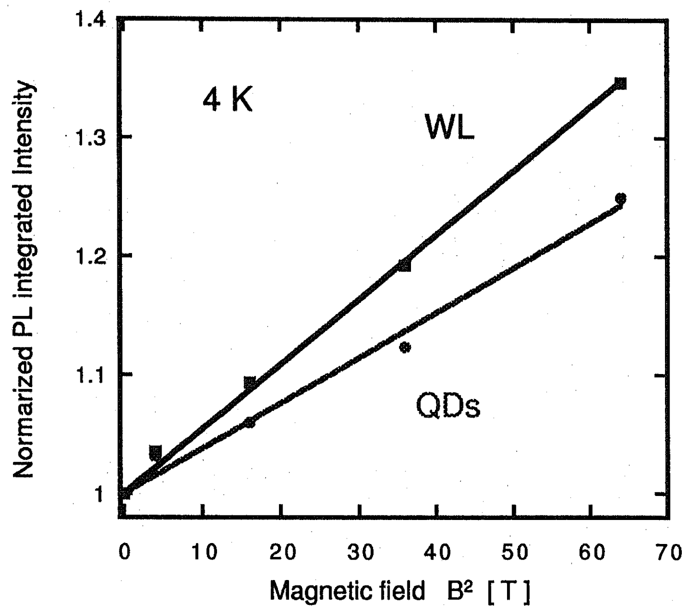

Fig. 5.4: Integrated intensity as a function of square of magnetic fields in a type-II GaSb/GaAs

Figure 5.4 shows The integrated intensity increases with magnetic fields. It is

mostly due to enhancement of the oscillator strength. Significant differences in the shifts between the quantum dots and the wetting layer were observed. The difference is caused by dimensions of confinement. The Coulomb attraction strongly enhances the oscillator strength and gives rise to a divergent Coulomb shift $\sim 1/r$ as compared to the size quantization effects $\sim 1/r^2$.[9, 10]

5.5 Exciton Binding Energy

In order to estimate the exciton binding energy, we adopt with the appropriate choice of a variational wave function. A spherical type-II dot with infinite barriers was assumed as shown in Fig. 5.5. The confined particle will not be altered by the Coulomb interaction since E (confinement) >> E (Coulomb) for infinite barriers. The unconfined or free particle will be affected by the Coulomb interaction and its wavefunction will peak near the dot and will be forced to vanish at r=a for infinite barriers. For infinite barriers we used a variation wave function of term[11, 12]

$$\begin{array}{ll} \psi_e(r_e) = (r_e - a)exp[-(r_e - a)\frac{b}{2}](\frac{2a^2}{b^3} + \frac{12a}{b^4} + \frac{24}{b^5})^{-1} & (r \geq a), \\ \psi_e(r_e) = 0 & (r < a), \end{array}$$

where b is the variational parameter which is $b = 2/a_0$, and a_0 is the effective orbital size. The minimization of this energy function with respect to the variational parameter b gives the binding energy and the wave function. Thus, it can be evaluated numerically. E_x is for the system assuming type-II infinite barriers.

Here the numerical results are presented. Figure 5.5 shows the calculated exciton binding energy in a type-II quantum dot as a function of dot diameters. For our GaSb/GaAs quantum dots, the exciton diameter, 12 nm, derived from the experimental diamagnetic shift is corresponding to the exciton binding energy ~12

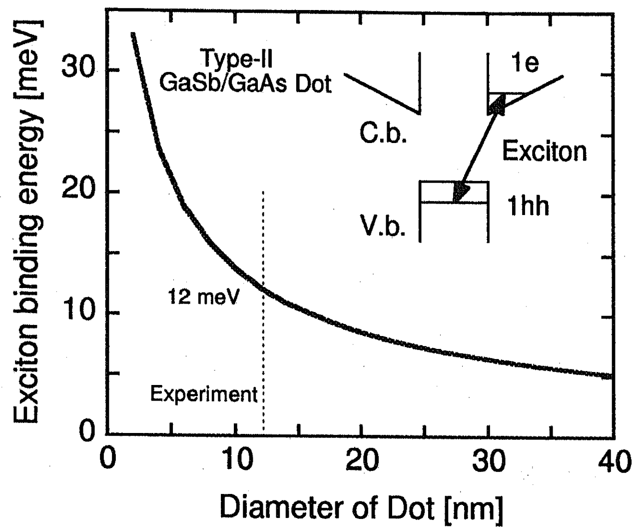

Fig. 5.5: The calculated exciton binding energy in a type-II quantum dot as a function of dot diameters.

meV. Compared with type-I quantum dots, it is about three times smaller than the exciton binding energy in a type-I dot which is ~37 meV.[4] However, it is as large as in a conventional GaAs/AlGaAs quantum well, even though the excitons is in type-II band alignment. Such large exciton binding energy is due to 3D confinement in a quantum dot.

5.6 Summary

In chapter V, we have performed a magneto-photoluminescence study on GaSb/GaAs quantum dots of a type-II band alignment. We have observed the diamagnetic shifts and the enhanced intensity with applied magnetic fields. We have explained that these effects are due to type-II band alignment. Also, the lateral quantum confinement in the GaSb/GaAs quantum dots was confirmed. In addition, the exciton biding energy in the type-II GaSb/GaAs quantum dots was extracted to be ~12 meV, compared with calculations and the experiment results.

Bibliography

[1] J. -Y. Marzin, J. M. Gerard, A. Izrael, D. Barrier, and G. Bastard, Phys. Rev. Lett. **73**, 716, (1994).

[2] S. Fafard, R. Leon, D. Leonard, J. L. Merz, and P. M. Petroff, Phys. Rev. **B50**, 8086, (1994).

[3] M. Grundmann, J. Christen, N.N. Ledentsov, J. Boehrer, D. Bimberg, S. S. Ruvimov, P. Werner, U. Richter, U. Goesele, J. Heydenreich, Y. M. Ustinov, A. Yu. Egorov, A. E. Zhukov, P. S. Kop'ev, and Zh.I. Alferov, Phys. Rev. Lett. **74**, 4043, (1995).

[4] P. D. Wang, J. L. Merz, S. Fafard, R. Leon, D. Leonard, G. Medeiros-Ribeiro, M. Oestreich, P. M. Petroff, K. Uchida, N. Miura, H. Akiyama, and H. Sakaki, Phys. Rev. B **53**, 16485, (1996).

[5] I. E. Itskevich, M. Henini, H. A. Carmona, L. Eaves, P. C. Main, D. K. Maude, and J. C. Portal, Appl. Phys. Lett. **70**, 505, (1997).

[6] M. Sugawara, Y. Nakata, K. Mukai, and H. Shoji, Phys. Rev. B **55**, 13155, (1997).

[7] Y. Toda, S. Shinomori, K. Szuuki, and Y. Arakawa, Appl. Phys. Lett. **73**, 517, (1998).

[8] K. Suzuki, R. A. Hogg, K. Tachibana, and Y. Arakawa, Jpn. J. Appl. Phys.**37** L203 (1998).

[9] G. W. Bryant, Phys. Rev. B **37**, 8763, (1988).

[10] R. Leon, S. Fafard, D. Leonard, J. L. Merz, and P. M. Petroff, Appl. Phys. Lett. **67**, 521, (1995).

[11] G.Bastard, *Wave Mechanics Applied to Semiconductor Heterostructures*, Les Editions de physique, France, 1992.

[12] J. M. Rorison, Physical Rev B **48**, 4643, (1993).

Chapter 6

Type-I InAs and Type-II GaSb Coupled Quantum Dots

6.1 Introduction

Recently, closely coupled InAs and InAs quantum dots in a GaAs have been performed.[1] A low energy shift and a decreasing full width at half maximum (FWHM) of the ground state photoluminescence in multiply stacked samples have been attributed to the formation of coherent superlattice-like states[2, 3] and the altered strain distribution in quantum dot stacked structures[4]. However, a study on coupled type-I and type-II quantum dots has not yet been reported, GaSb/GaAs self-assembled quantum dots (QDs) have been realized by molecular beam epitaxy.[5, 6] GaSb/GaAs quantum dots should exhibit a type-II band alignment in real space. In this case, holes are localized within the GaSb quantum dots, while due to Coulomb attraction the electrons form a shell around quantum dots.[7, 8] Therefore, it allows a study on coupled quantum dots with *band structure engineering.*

In this chapter, we investigate optical properties of closely coupled InAs and GaSb self-assembled quantum dots in a GaAs. Photoluminescence (PL) from coupled quantum dots of a type-I and a type-II band alignment is observed. In addition,

we study that the energy shifts of these peaks for various excitation intensity strongly depended on the interval layer thickness between each coupled quantum dots.

6.2 Epitaxial Growth of Coupled Quantum Dots

Stacked structures of self-assembled GaSb and InAs quantum dots in a GaAs were grown by molecular beam epitaxy. The substrate temperature was 450 °C while formation of each self-assembled quantum dots, GaAs interval layer, and GaAs capped layer were deposited. See chapter II about the detail growth condition.

In multi-layered samples, the surface stress introduced in the capping layer by an initial set of buried islands leads to stress-directed ad-atom migration and hence vertical self-organization of island stacks.[9] The quantum dot shape is determined to be minimized during the formation of quantum dots and the deposition of capping layer. Then the shape of quantum dots was changes while it is capped.[10]

6.3 Photoluminescence of InAs and GaSb Quantum Dots

These vertically aligned quantum dots have been designed to be vertically connected and electronically coupled. The weak coupling state produces small changes in spectral peak position and linewidth. Photoluminescence measurements were performed by pumping He-Ne laser at 20 K.

Figure 6.1 shows PL spectra with varying excitation intensity on GaSb and InAs coupled quantum dots. PL peaks at ~1.3 eV and ~1 eV were from InAs quantum dots and GaSb quantum dots. Since an oscillator strength in a type-II is smaller than that in a type-I, emission from type-II quantum dots is much smaller.

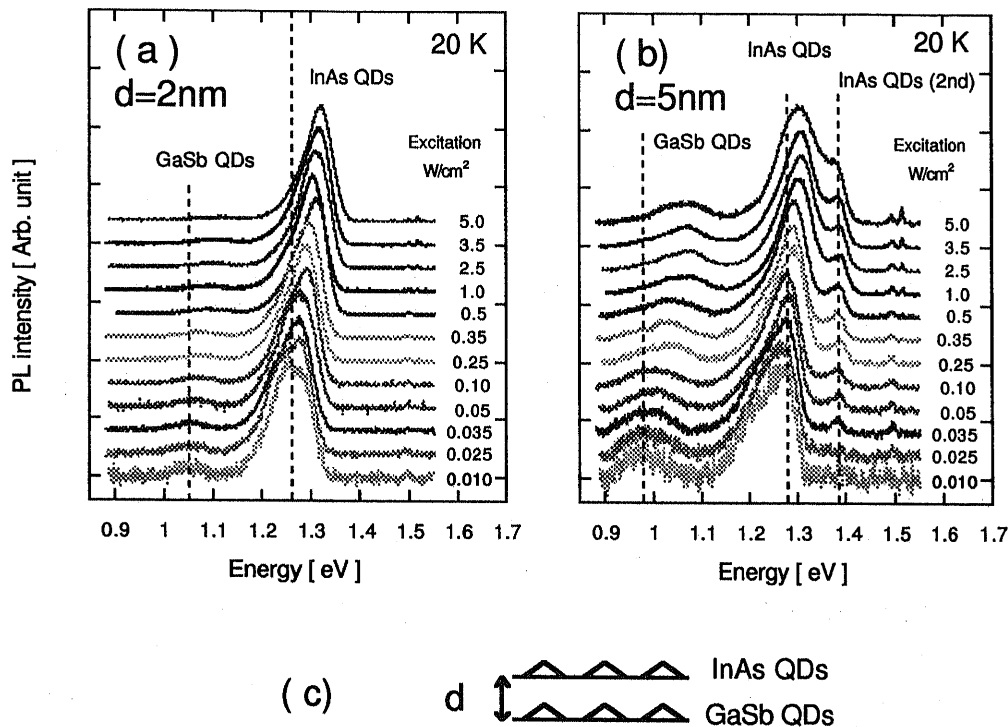

Fig. 6.1: PL spectra with varying excitation intensity on GaSb and InAs coupled quantum dots. Where d means an interval layer thickness of GaAs between each quantum dots. (a) and (b) show on samples with the different interval layer thickness of 2 and 5 nm, respectively. (c) shows a schematic drawing of the sample structure.

Where d means the interval layer thickness of GaAs between each quantum dots. In the sample d = 2 nm, PL intensity of GaSb is considerably weak. It indicates the relaxation of carriers to InAs quantum dots.

These peaks of PL shifted towards higher energies with increasing excitation intensity. However, these behaviors depended on the interval layer thickness. Figure 6.2 shows energy shifts of each PL peaks as a function of excitation intensity on GaSb and InAs coupled quantum dots. In particular, shifts in the closer sample

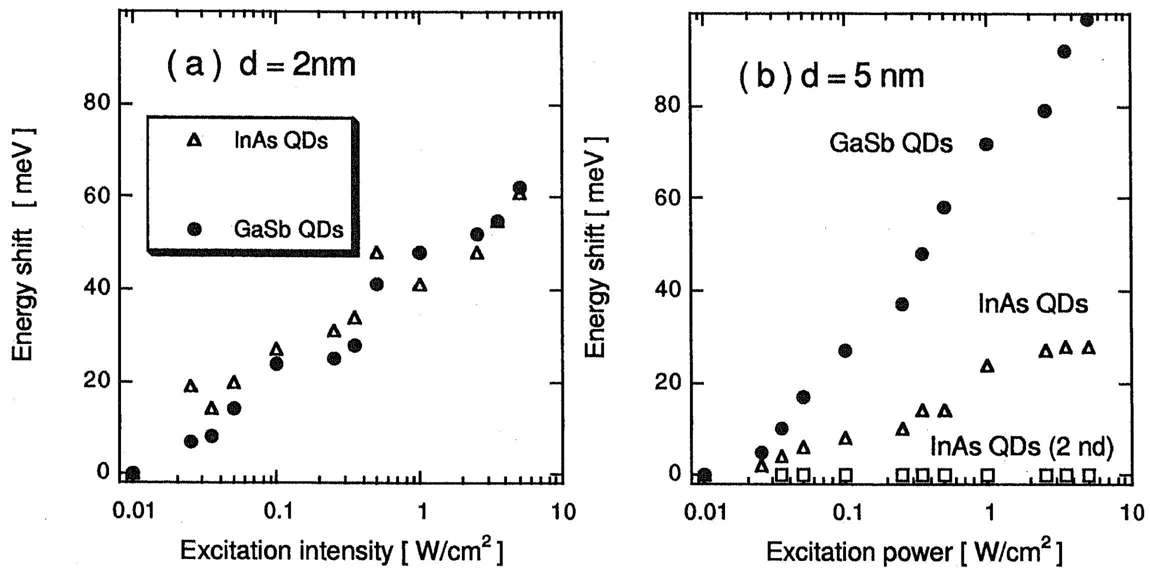

Fig. 6.2: Energy shifts of each PL peaks as a function of excitation intensity on GaSb and InAs coupled quantum dots. (a) and (b) show on samples with the different interval layer thickness of 2 and 5 nm, respectively.

(d = 2 nm) are due to the interaction between type-I and type-II quantum dots. Carriers tunnel thorough the vertical barriers.

Figure 6.3 shows a schematic band diagram of coupled quantum dots. In this case of the closer sample, electrons around GaSb quantum dots coupled ones in InAs quantum dots were realized. Therefore, there was no peak of InAs 2nd state in the closer sample. We will discuss further details in the conference.

The decrease can be explained as quantum tunneling of electrons through barriers. These results indicate that the tunneling mechanism dominates reduction of

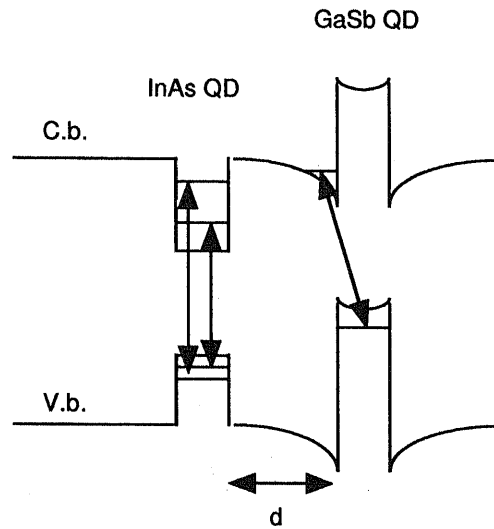

Fig. 6.3: A schematic band diagram in a type-II GaSb and Type-I InAs coupled quantum dots.

the overlap of the wavefunction between electrons and holes. However, we note the quantum dots are connected through the wetting layer. In addition, we suppose a device application using this system. we can make use of the size distribution of the quantum dots for optical memory. It is useful for a multi-wavelength optical memory. It is read through a charge in the conductivity of two-dimensional electron gas located closely on the quantum dots.

6.4 Summary

In chapter VI, we have investigated optical properties on coupled quantum dots of a type-I and a type-II band alignment. Different behaviors were obtained in structures with varying the interval layer thickness. It is due to an interaction between type-I and type-II quantum dots.

Bibliography

[1] Y. Sugiyama, Y. Nakata, T. Futatsugi, M. Sugawara, Y. Awano, and N. Yokohama, Jpn. J. Appl. Phys. **36**, L-158, (1997).

[2] G. S. Solomon, J. A. Trezza, A. F. Marshall, and J. S. Harris, Phys. Rev. B.**76** 952 (1996).

[3] N. N. Ledentsov, V. A. Shchukin, M. Grundmann, N. Kirstaedter, J. Böhrer, O. Schumidt, D. Bimberg, V. M. Ustinov, A. Y. Egorov, A. E. Zhukov, P. S. Kop'ev, S. V. Ruvimov, P. Werner, U. Gösele, and J. Heydenreich, Phys. Rev. B.**54** 8743 (1996).

[4] R. Heitz, A. Kalburge, Q. Xie, M. Grundmann, P. Chen, A. Hoffmann, A. Madhukar, and D. Bimberg, Phys. Rev. B.**57** 9050 (1998).

[5] K. Suzuki, R. A. Hogg, K. Tachibana, and Y. Arakawa, Jpn. J. Appl. Phys. **37**, L-203, (1998).

[6] C. -K.Sun, G. Wang, J. E. Bowers, B. Brar, H. -R. Blank, H.Kroemer, and M.H.Pilkuhn, Appl. Phys. Lett. **68** 1543 (1996).

[7] F. Hatami, M. Grundmann, N. N. Ledentsov, F. Heinrichsdorff, R. Heitz, J. Böhrer, D. Bimberg, S. S. Ruvimov, P. Werner, V. M. Ustinov, P. S. Kop'ev, and Zh. I. Alferov, Phys. Rev. B.**57** 4635 (1998).

[8] R. A. Hogg, K. Suzuki, K. Tachibana, L. Finger, K. Hirakawa, and Y. Arakawa, Appl. Phys. Lett. **72** 2856 (1998).

[9] Q. Xie, A. Madhukar, P. Chen, and N. P. Kobayashi, Phys. Rev. Lett.**75** 2542 (1995).

[10] J. M. Garcia, T. Mankad, P. O. Holtz, P. J. Wellman, and P. M. Petroff, Appl. Phys. Lett. **72** 3172 (1998).

Chapter 7

InSb/GaSb Self-assembled Dots

7.1 Introduction

InSb/GaSb quantum dots have a possibility for optical devices in mid-IR region. Besides, it has type-I band alignment and the lightest effective mass in III-V compounds. Therefore, the InSb/GaSb are currently topics of great interest. However, GaSb layer has a large lattice mismatch on a GaAs substrate. It is required to grow high quality GaSb buffer layers on a GaAs.

In this chapter, we grow GaSb buffer layers on a GaAs with a superlattice. The GaSb surface is characterized by atomic force microscopy (AFM). We investigate the effect of a superlattice for the surface roughness, and expect to grow a perfect flat surface in our optimized epitaxial growth condition. In addition, InSb/GaSb dots are also grown.

7.2 Epitaxial Growth of GaSb Buffer Layers on GaAs with a Superlattice

A GaSb layer on a GaAs is expected to be compressively strained due to a lattice mismatch of 7.8 %. A surface roughness can be directly related to interface roughness for heterostructure devices. The goal of this material study was the production of a high-quality relaxed buffer layer on GaAs. This was partially overcome by growing a thick buffer layer of GaSb or AlSb on a GaAs. The heteroepitaxy is subject to grow spirally from a screw dislocation.[1, 2]

In this system, D. H. Chow *et al.* found to improve the structural quality of the buffer layer with a superlattice.[3] In this work, we use atomic force microscopy to obtain detailed topological information of the surface.

All samples studied were grown on semi-insulating (001) GaAs substrates using VG 80 MBE system equipped with elemental sources for group III and V materials. The antimony source was uncracked Sb_4, and a valved cracker cell was employed to produce As_2.

Sample structures

In order to overcome the large strain, we employed a GaSb/GaAs superlattice on the GaAs layer before a thick GaSb layer. Figure 7.1 shows a schematic drawing of sample structures. Figure 7.1 (a) and (b) show structures without a superlattice buffer layer and with one. The superlattice buffer layer, $(GaSb)_1$ $(GaAs)_1$ consists of 1 monolayer (ML) GaSb followed by 1 ML GaAs, periodically repeated.

In addition to a superlattice buffer layer, an AlSb buffer layer was used as shown

in Fig. 7.1 (c). The purpose of the AlSb nucleation layer is to help smooth growth at the lattice mismatched interface. This is because spiral growth is not initiated at the misfit dislocation due to the short diffusion length of the Al adatom.[1]

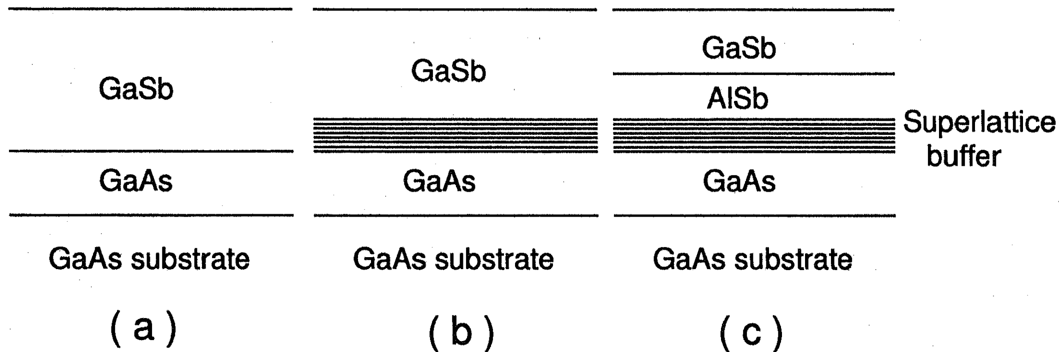

Fig. 7.1: A schematic drawing of sample structures. (a) without a superlattice buffer layer. (b)with one. (c)In addition to the superlattice, an AlSb buffer was also used.

Epitaxial Growth Conditions

After oxide desorption, a GaAs buffer of was grown at 580°C on a GaAs semi-insulating (001) substrate. For the sample a and b, the growth temperature of 400°C and 380°C are used for the GaSb/GaAs superlattice layer and GaSb thick buffer layer, respectively. The growth rates of 0.21 nm/s for GaSb and 0.17 nm/s for GaAs were used. Then the Sb/Ga beam equivalent pressure (BEP) ratio was 5.

On the other hand, for the sample c, the growth temperature of 550°C are used for the GaSb/GaAs superlattice layer, AlSb layer, and GaSb thick buffer layer. The growth rates of 0.07 nm/s for GaSb, 0.06 nm/s for AlSb, and 0.06 nm/s for GaAs

were used. Then the Sb/Ga BEP ratio was 10. Compared to the sample (a) and (b), higher temperature and slower growth rates were employed in the sample (c).

7.3 Surface Morphology of GaSb Buffer Layers on GaAs with a Superlattice

The GaSb surface is characterized by atomic force microscopy. Here, The surface roughness is defined as

$$[\Sigma(h_i - \bar{h})^2/N]^{1/2}$$

where h_i is the height, $\bar{h}$ is the mean and the sum is over all image data points N.

The effect of a superlattice

A comparison of the surface with a superlattice buffer layer and without one is shown in Fig. 7.2. We observed a significant difference between the two samples. A comparison of the surface morphology indicates the effect of a superlattice. In particular, on the cross section along $\langle 110 \rangle$ the surface was improved. This is attributed to Ga migration.

The growth parameters and the observed surface roughness of a series of GaSb buffer layers are given by in Table 7-1. The surface have different surface roughness. These features are always associated with the effect of the superlattice. Obviously the surface grown at 550°C is most suitable rather than those at 380°C. The surface roughness was reduced by adequate growth temperature. As a result, a flat surface less than the 1 ML was obtained in our optimized epitaxial growth condition in the sample A7.

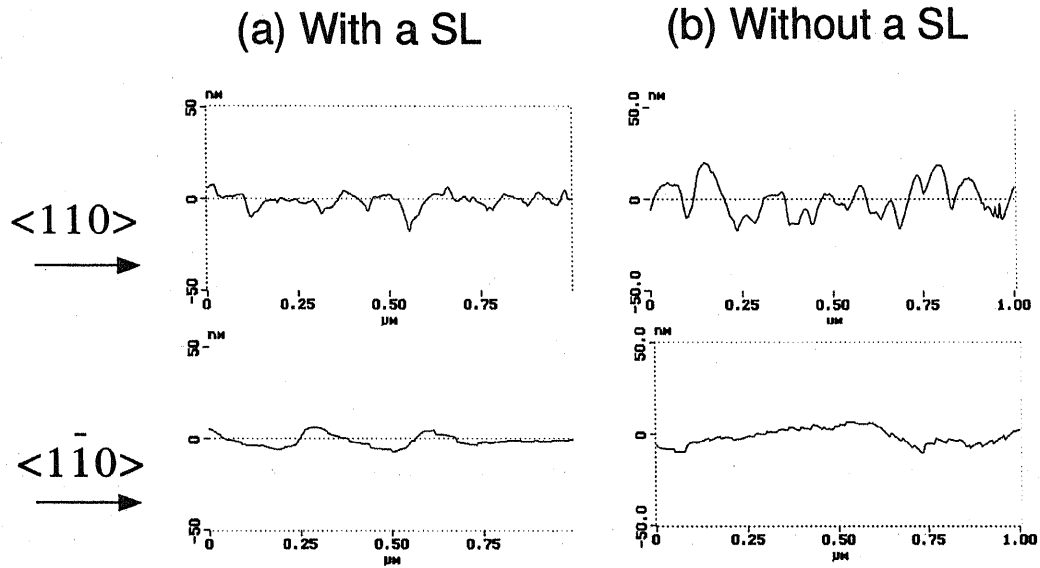

Fig. 7.2: Cross section on the surface. (a) with a superlattice buffer layer (Sample A2). (b)without one (Sample A1).

Sample	Structure	Temp.	SL periods	GaSb thickness (μm)	Surface roughness (nm)
A1	a (without a SL)	380	0	3	8
A2	b	380	200	3	5
A3	b	380	10	1	8
A4	b	380	100	2	6
A5	b	380	200	2	5
A6	c (without a SL)	550	0	0.3	1.4
A7	c	550	100	0.3	1

Table 7-1 : The growth parameters of a series of GaSb buffer layer and the surface roughness. The structure is corresponding to Fig.7.1.

7.4 Strain in a GaSb/GaAs Superlattice

The strain inside a $(GaSb)_1(GaAs)_1$ superlattice is calculated. We use the keating potential[4] to minimize the strain energy in a tetrahedral unit cell. The strain energy E is express as

$$E = \frac{1}{2}\sum_{i(j)} \frac{3\alpha}{8d_0^2}\left(|\boldsymbol{x}_i - \boldsymbol{x}_j|^2 - d_0^2\right)^2 + \sum_{i(j,k)} \frac{3\beta}{8d_0^2}\left[(\boldsymbol{x}_j - \boldsymbol{x}_i)\cdot(\boldsymbol{x}_k - \boldsymbol{x}_i) + \frac{1}{3}d_0^2\right]^2,$$

where d_0 is the equilibrium bound length, $\boldsymbol{x}_i$ is the atomic position of the i-th atom, and α and β are the bound-stretching and the bound-bending force constants, respectively. The first sum is over all atoms i and their four neighbors j. The second sum is over all atoms i and all pairs of their neighbors j and k. We use $d_0 = 0.305$ nm, $\alpha = 33.16\times 10^3$ dyn/cm and $\beta = 7.22\times 10^3$ dyn/cm for a GaSb, and $d_0 = 0.283$ nm, $\alpha = 41.19\times 10^3$ dyn/cm and $\beta = 8.95\times 10^3$ dyn/cm for a GaAs, respectively.

The GaSb/GaAs has a large mismatch (7.8 %). Even a $GaSb_{0.5}As_{0.5}$/GaAs has half of one (3.9 %). However, the $(GaSb)_1(GaAs)_1$ has small mismatch (0.92 %) As shown in Table 7.2, the calculation result supports the effect of the superlattice buffer layer.

Materials	Strain(%)
GaSb/GaAs	7.8
$GaSb_{0.5}As_{0.5}$/GaAs	3.9
$(GaSb)_1/(GaAs)_1$	0.92

Table 7.2 : Calculated strain in a superlattice. This results indicate the effect of a superlattice buffer layer.

7.5 Epitaxial Growth of InSb/GaSb Dots

Introduction

InSb/GaSb quantum dots have a possibility for optical devices in mid-IR region. Besides, the InSb/GaSb quantum dots have type-I band alignment and the lightest effective mass in III-V compounds. Therefore, the InSb/GaSb and InSb/AlGaSb are currently topics of great interest.[5, 6, 7]

Epitaxial growth conditions

A *GaSb* substrate (001) was used. After it was deoxiced, 50 nm GaSb buffer layer was deposited. An InSb of 2 ML was grown on a GaSb. We decide 2 ML deposition, since Yano *et al.* reported that InSb deposition does not increase the density and reached a saturation at $\sim 10^8$ cm^{-8}, corresponding to the thickness from 2 ML to 6 ML.[7] The deposition was performed at low temperature. The growth rate and the Sb/In ratio of InSb are 0.029 monolayers/s and 10, respectively. The sample structure is shown in Fig. 7.3.

InSb dots

The grown sample was characterized by atomic force microscopy (AFM). Figure 7.3 shows AFM image of 2 ML InSb on a GaSb. Figure 7.3 (b) (1μm$\times 1\mu$m) and (c) (5μm$\times 5\mu$m) show AFM images of InSb dot grown at 250°C and 380°C, respectively. The InSb dots at 250°C heve a diameter and a density are 80 nm and $\sim 10^9$, respectively. On the other hand, the InSb dots at 380°C heve a diameter and a density are 300 nm and $\sim 10^8$, respectively. As the growth temperature is lowered, the dot diameter becomes small. This behavior is consistent with another self-assembled dots. However, the temperature of 250°C seems to be not enough to form *quantum* dots with a lateral confinement. One of the reasons is due to the low

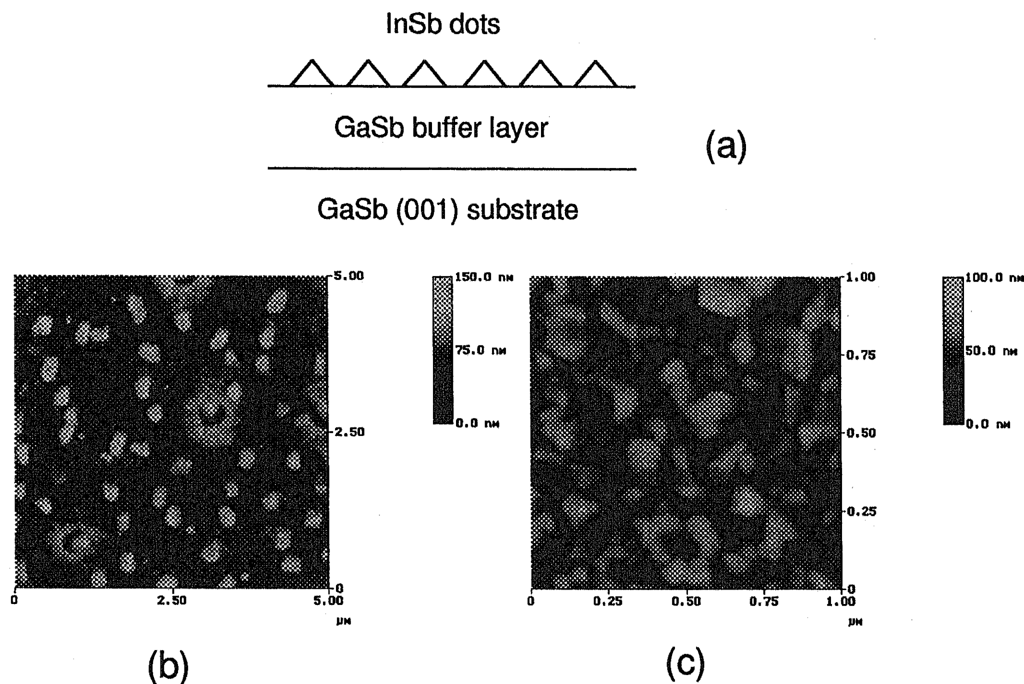

Fig. 7.3: (a) A schematic drawing of sample structure. (b) ($1\mu m \times 1\mu m$) and (c) ($5\mu m \times 5\mu m$) show AFM images of InSb dot grown at 250°C and 380°C, respectively.

binding energy of the In-Sb bond is 1.40 eV. It is smaller than that of the In-As (1.55 eV). This contributes to form self-assembled dots. Therefore, the InSb/GaSb dots are formed at low temperature.

However, the dot diameter is one order of magnitude larger and the dot density is two orders of magnitude lower than that for GaSb/GaAs quantum dots.[8] The InSb dots easily become large size. As a results, the lateral size of InSb/GaSb dots are too large to confine electrons and holes in a three-dimension quantum dot.

7.6 Summary

In chapter VII, we have grown GaSb buffer layers on a GaAs with a superlattice. The GaSb surface was characterized by atomic force microscopy. The surface roughness was reduced by the effect of a superlattice. As a result, a flat surface less than the 1 nm was obtained in our optimized epitaxial growth condition. In addition, InSb/GaSb dots have also grown.

Bibliography

[1] B. Brar and D. Leonard, Appl. Phys. Lett. **66**, 463 (1995).

[2] S. J. Brown, M. P. Grimshaw, D. A. Ritchie, and G. A. Jones, Appl. Phys. Lett. **69**, 1468 (1996).

[3] D. H. Chow, R. H. Miles, J. R. Sŏderströme, and T. C. McGill, J. Vac. Sci. Technol. B, **8**, No.4 710 (1990).

[4] P. N. Keating, Phys. Rev. **145**, 637, (1966).

[5] N. Bertru, O. Brandt, M. Wassermeier, and K. Ploog, Appl. Phys. Lett. **71**, 193 (1997).

[6] A. F. Tsatsul'nikov, N. N. Ledensov, M. V. Maksimov, B. Ya. Mel'tser, P. V. Nekludov, S. V. Shaposhinkov, B. V. Volvik, I. L. Krestnikov, A. V. Sakharov, N. A. Bert, P. S. Kop'ev, Zh. I. Alferov, and D. Bimberg, Semiconductor **31**, 55, (1997).

[7] M. Yano, Y. Seki, H. Ohkawa, K. Koike, S. Sasa, and M. Inoue, Jpn. J. Appl. Phys. **37**, 2455, (1998).

[8] K. Suzuki, R. A. Hogg, K. Tachibana, and Y. Arakawa, Jpn. J. Appl. Phys.**37** L203 (1998).

Chapter 8

Conclusions

8.1 Summary

In this thesis, epitaxial growth and their optical properties of self-assembled GaSb quantum dots were investigated. *Band structure engineering* was realized in quantum dots.

In chapter I, the background of research on quantum dots was described. In addition, band alignment in real space and device applications of a GaSb were explained. Objective and scope of present works were mentioned.

In chapter II, epitaxial growth of self-assembled GaSb quantum dots on a GaAs using the Stranski-Krastanow mode have described. The growth mechanism are discussed in detail. Consequently, the average diameter and height of the quantum dots are 26 nm and 6.2 nm, respectively. Moreover, the density was systematically controlled between 2.6×10^9 to 1.2×10^{10} cm^{-2} by carefully choosing the amount of deposited GaSb from 2.5 to 3.1 monolayers. In addition, a stacked structure of self-assembled GaSb/GaAs quantum dots with nanometer-scale dimensions also were grown. These results are very useful in forming a quantum dot of staggered band lineup (type-II) of possible use in novel device applications.

In chapter III, the features in photoluminescence (PL) measurements from the quantum dots were observed at ~1.1 eV, clearly separated from that of the wetting layer at ~1.3 eV. This result indicates that we have achieved control of As-Sb intermixing in GaSb/GaAs heterostructure despite the deposition of only a few monolayers of material. With increasing excitation intensity, the peak from the quantum dots shifted towards higher energies, with a shift 6.5 times larger than that of the peak from the wetting layer. It is due to increased charge density. The results are consistent with a type-II band alignment. In temperature dependence of photoluminescence measurements, we observed a thermal activation energy of 130 meV for the quantum dots luminescence indicating strong localization of excitons in the quantum dots. photoluminescence excitation measurements have confirmed our assignment of the quantum dot related peaks and a feature 25-27 meV higher in energy than the detection energy has been discussed in terms of phonon relaxation.

In chapter IV, we have performed time-resolved PL measurements on the type-II GaSb/GaAs self-assembled quantum dots grown. The dynamic behavior of the quantum dots and the wetting layer was systematically investigated. The radiative lifetimes (~23 ns) in the quantum dots were considerably longer than those in type-I quantum dots. The initial decay was shortened with increasing excitation intensity. This is attributed to spatially indirect excitons in the type-II band alignment. In addition, a conduction band discontinuity of the quantum dots was discussed. The offset of ~50 meV was extracted.

In chapter V, we have performed a magneto-photoluminescence study on the type-II GaSb/GaAs quantum dots We have observed the diamagnetic shifts and the enhanced intensity with applied magnetic fields. We have explained that the be-

havior is due to the type-II band alignment. Also, the lateral quantum confinement in the GaSb/GaAs quantum dots was confirmed. In addition, the exciton biding energy in the type-II GaSb/GaAs quantum dots was extracted to be ~12 meV, compared with calculations and the experiment results.

In chapter VI, we have investigated optical properties on coupled quantum dots of a type-I and a type-II band alignment. Different behavior was obtained in structures with varying the interval layer thickness. It is due to an interaction between type-I and type-II quantum dots.

In chapter VII, we have grown high quality GaSb buffer layers on a GaAs with a superlattice. The GaSb surface was characterized by atomic force microscopy. The surface roughness was reduced by the effect of a superlattice. In our optimized epitaxial growth condition, the flat surface less than 1 nm was obtained. In addition, InSb/GaSb dots have also grown.

8.2 Future Prospect

In this work, epitaxial growth and their optical properties of self-assembled GaSb quantum dots were revealed. The future applications of the quantum dots are limited only by physics. The author hopes that the these research contributes to the fundamental understanding of the quantum dots and application to novel optical devices.

There is also the possibility of useful applications as this system has a band gap in the 1 - 5 μm region, useful for optical devices, such as infrared lasers and detector.

Appendix A

Photoluminescence of Nonequilibrium Carriers in Type-II Band Alignment

A nonexcitonic mechanism of a nonequilibrium carrier recombination being indirect in real space has to be considered in view of the observed high luminescence efficiency.[1] The formation of a dipole layer populated with quantized nonequilibrium carriers close to the GaSb/GaAs interface at even moderate excitation intensities is responsible for this effect. The attractive potential of this layer forms a quantum well for nonequilibrium electrons, the quantization energy of which depends on the excitation intensity. An increase in the excitation density raises the steepness of the confining potential and, consequently, the electron quantization energy.[2]

The steady-state sheet concentrations of electrons n_W and holes p_W generated in the thin layer region by a photon flux I are characterized by the relation

$$n_W \, p_W = n_W^2 = \frac{\alpha I (L + l)^2}{\gamma}.$$

Here a denotes the absorption coefficient, L the width of the GaSb layer, l the multiple-quantum-well cladding layer thickness, and γ the radiative recombination coefficient. The strongly localized holes form a charged plane and, correspondingly,

produce an approximately triangular well with an electric-field strength of

$$\varepsilon = \frac{2\pi e n_W}{\varepsilon_0} \propto \sqrt{I}.$$

The ground electron state in such a well is given by[3]

$$E_e = const\, \varepsilon^{2/3} \equiv b I^{1/3},$$

with

$$b = \left(\frac{9\pi}{8}\right)^{2/3} \left(\frac{\hbar^2}{2m_e}\right)^{2/3} \left(\frac{\alpha(L+l)^2}{\gamma}\right)^{1/3}.$$

The electron quantization energy is thus expected to increase proportionally with the third root of the excitation density.

Bibliography

[1] N. N. Ledentsov, J. Böhrer, M. Beer,F. Heinrichsdorff, M. Grundmann, D. Bimberg, S. V. Ivanov, B. Ya. Meltser, S. V. Shaposhnikov, I. N. Yassievich, P. S. Kop'ev, and Zh. I. Alferov, Phys. Rev. **B52** 14058 (1995).

[2] M. S. Bressler, O. B. Gusev, M. P. Mikhailova, V. V. Sherstnev, Yu. P. Yakovlev, and I. N. Yassievich, Fiz. Tekh. Polopruvodn. **25**, 298, (1991). [Sov. Phys. Semicond. **25**, 181, (1991)]

[3] C. Weisbuch, and B. Vinter, *Quantum Semiconductor Structures*, (Academic, Boston, 1991), p.20.

Appendix B

Material Parameters of Gallium Antimonide

B.1 Temperature dependence of the energy gaps

Compound	Type	Bandgap 0 K	Eg(eV) 300 K	Temperature deoendence of bandgap $Eg(T)$ (eV)
AlSb	Indirect(X)	1.687	1.58	$1.687 - 4.97 \times 10^{-4}T^2/(T + 213)$
GaAs	Direct(Γ)	1.519	1.424	$1.519 - 5.405 \times 10^{-4}T^2/(T + 204)$
GaSb	Direct(Γ)	0.810	0.726	$0.810 - 3.78 \times 10^{-4}T^2/(T + 94)$
InAs	Direct(Γ)	0.420	0.360	$0.420 - 2.50 \times 10^{-4}T^2/(T + 75)$
InSb	Direct(Γ)	0.236	0.172	$0.236 - 2.99 \times 10^{-4}T^2/(T + 140)$

Table B.1 Temperature dependence of the energy gaps of several semiconductor alloys.(From Casey and Panish [1])

B.2 Effective masses and dielectric constants

Compound	Electron mass m_e^*	Hole mass m_{hh}^*	Dielectric constant (ε_0)
AlSb	0.12	0.98	14.4
GaAs	0.067	0.45	13.1
GaSb	0.042	0.4	15.7
InAs	0.023	0.4	14.6
InSb	0.0145	0.4	17.7

Table B-2 : Effective masses and dielectric constants.
(From Casey and Panish [1])

B.3 Material properties of GaSb

Property	Value
Lattice constant (nm)	0.60959
Density (gm cm^{-3})	5.6137
Melting point (K)	985
Debye temperature (K)	266
Coefficient of thermal expansion (10^{-6}°C^{-1}) at 300 K	7.75
Thermal conductivity at 300 K (W cm^{-1} K^{-1})	0.39
Direct energy gap at 300 K (eV)	0.725
Direct energy gap at 0 K (eV)	0.822
Temperature dependence of minimum energy gap ($\times 10^{-4}$ eV K^{-1})	
α	4.2
β	140
Spin-orbit splitting energy, Δ_0 (eV)	0.80
Effective mass of electrons (in units of m_0)	0.0412
Effective mass of holes (in units of m_0)	
Heavy hole mass	0.28
Light hole mass	0.05
Spin-orbit split mass	0.13
Wave number of LO phonons (cm^{-1})	233.0
Wave number of TO phonons (cm^{-1})	224.0
Refractive index (near band-gap energy)	3.82
Dielectric constant	
ϵ_0	15.69
ϵ_∞	14.44
Elastic compliances ($\times 10^{-12}$ cm^2 dyn^{-1})	
S_{11}	1.582
S_{12}	-0.495
S_{44}	2.314
Deformation potential constants (for direct gap)	
a (eV)	-8.28
b (eV)	-2.0
d (eV)	-4.7

Table B.3 : Material properties of GaSb (from Ref.[2])

B.4 Compositional dependence of the energy gaps

Compound	Direct energy bandgap Eg (eV)
$Al_xGa_{1-x}Sb$	$0.726 + 1.129\ x + 0.368\ x^2$
$Al_xIn_{1-x}Sb$	$0.172 + 1.621\ x + 0.43\ x^2$
$Ga_xIn_{1-x}Sb$	$0.172 + 0.139\ x + 0.415\ x^2$
$GaAs_xSb_{1-x}$	$0.726 - 0.502\ x + 1.2\ x^2$
$InAs_xSb_{1-x}$	$0.18 - 0.41\ x + 0.58\ x^2$

Table B.4 : Compositional dependence of the energy gaps in several semiconductor alloys at 300 K.(From Casey and Panish [1])

B.5 Band structure of GaSb

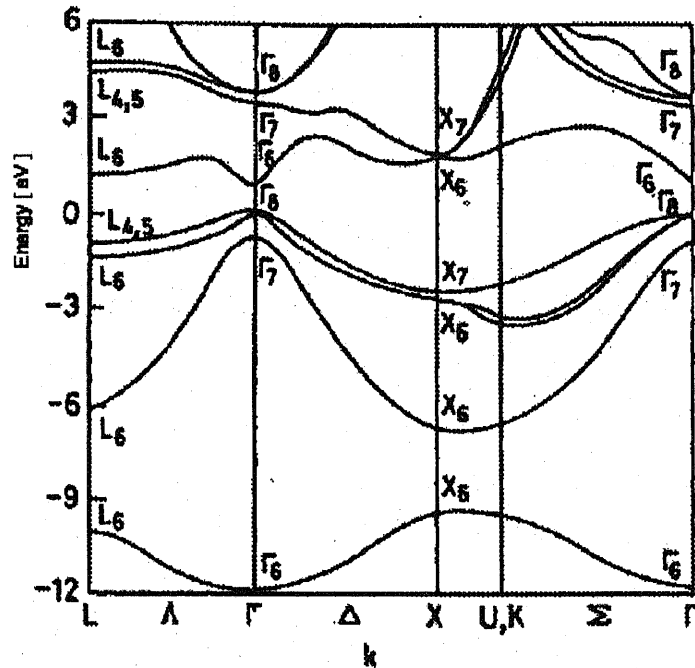

Fig. B.1: Band structure of GaSb (from Ref. [3])

Bibliography

[1] C. H. Casey, Jr. and M. B. Panish, *Heterostructure Lasers, Part A, Fundamental Principles and Part B, Material and Operating Characteristics* ,Academic Press, New York, 1978.

[2] P. S. Dutta, H. L. Bhat, and V. Kumar, J. Appl. Phys. (Applied Physics Review) **81**, 5821 , (1997).

[3] J. R. Chelikowsky and M. L. Cohen, Phys. Rev. B **14**, 556, (1976).

Publications

(1) Journals

[1.1] K.Suzuki, R.A.Hogg, K.Tachibana, and Y.Arakawa
"Density Control of GaSb/GaAs Self-assembled Quantum Dots(~25nm) Grown by Molecular Beam Epitaxy"
Japanese Jounal of Applied Physics, **Vol.37**,No.2B., p.L203-L205,(1998).

[1.2] R.A.Hogg, K.Suzuki, K.Tachibana, L.Finger, K.Hirakawa, and Y.Arakawa
"Optical Spectroscopy of Self-assembled Type II GaSb/GaAs Quantum Dot Structures Grown by Molecular Beam Epitaxy"
Applied Physics Letters, **Vol.72**, p.2856-2858 (1998).

[1.3] K.Suzuki and Y.Arakawa
"Growth of Stacked GaSb/GaAs Self-assembled Quantum Dots by Molesular Beam Epitaxy"
To be published in Journal of Crystal Growth

[1.4] K.Suzuki, R.A.Hogg, and Y.Arakawa
"Structural and Optical Properties of Self-assembled Type-II GaSb/GaAs Quantum Dots Grown by Molecular Beam Epitaxy"
Submitted to Jounal of Applied Physics

[1.5] K. Suzuki, R. A. Hogg, S. Kako, Y. Arakawa, M. S. Minsky, S. B. Fleischer, E. Hu, and J. E. Bowers
"Radiative lifetimes of spatially indirect excitons in type-II GaSb/GaAs self-assembled quantum dots"
Submitted to Applied Physics Letters

[1.6] Y. Toda, S. Shinomori, K. Suzuki and Y. Arakawa
"Near-field Magneto-optical Spectroscopy of Single Self-assembled InAs

Quantum Dots"
Applied Physics Letters, **Vol.73**, p.517-519 (1998).

[1.7] K. Yamanaka, K. Suzuki, S. Ishida, and Y. Arakawa
"Light Emission from Individual Self-Assembled InAs/GaAs Quantum Dots Excited by Tunneling Current Injection"
Applied Physics Letters, **Vol.73** p.1460-1462 (1998).

[1.8] K. Yamanaka, S. Ishida, K. Suzuki, H. Hayashi, H. Watabe, and Y. Arakawa
"Light Emission from Individual InAs/GaAs Self-Assembled Quantum Dots Excited by Tunneling Current Injection"
Solid-State Electronics, **Vol.42**, p.1079-1082, (1998).

[1.9] Y. Toda, S. Shinomori, K. Suzuki, M. Nishioka, and Y. Arakawa
"Near-field Optical Spectroscopy of Self-assembled Quantum Dots : NSOM Apparatus for Measuring the Features of Single Dots"
Solid-State Electronics, **Vol.42**, p.1083-1086, (1998).

[1.10] Y. Toda, S. Shinomori, K. Suzuki, and Y. Arakawa
"Polarized photoluminescence spectroscopy of single self-assembled InAs quantum dots"
Physical Review B, **Vol.58**, p.R 10 147 - 10 150 (1998).

[1.11] K. Iizuka, K. Matsumaru, T. Suzuki, H. Hirose, K. Suzuki, and H. Okamoto
"Arsenic-free GaAs substrate preparation and direct growth of GaAs / AlGaAs multiple quantum well without Buffer Layer"
Journal of Crystal Growth **Vol.150** p.13-17 (1995)

(2) International conference

[2.1] K.Suzuki, M.S.Minsky, S.B.Fleisher, R.A.Hogg, J.E.Bowers, and Y.Arakawa
"Radiative Lifetime of Spatially Indirect Exciton in Type-II GaSb/GaAs Self-assembled Quantum Dots"
25th International Symposium on Compound Semiconductors (ISCS'98), Nara, Japan, 1998 October.

[2.2] K.Suzuki and Y.Arakawa
"Stranski-Krastanow Growth of Stacked GaSb/GaAs Qunatum Dots by Solid Source Molecular Beam Epitaxy"
10th International Conference on Molecular Beam Epitaxy (MBE-X), Cannes, France, 1998 September.

[2.3] K.Suzuki, R.A.Hogg, K.Tachibana, and Y.Arakawa
"Growth and Optical Properties of Self-assembled Type II GaSb/GaAs Quantum Dots"
Indium Phoshide and Related Materials (IPRM'98), Tsukuba, Japan, 1998, May

[2.4] K.Suzuki and Y.Arakawa
"Optical Properties of Type-I InAs and Type-II GaSb Coupled Quantum Dots"
Submitted to Optical Society of America (OSA'99) topical meeting, Colorado, U.S.A., 1999, April

[2.5] K. Suzuki, Y. Nagamune, H. Watabe, T. Noda, Y. Ohno, H. Sakaki, and Y. Arakawa
"Imaging of Hole Dynamics in Two-dimensional Electron Gas Systems using a Micro-photoluminescence: Temperature and Hole Concentration Dependence "
Pacific Rim Conference on Laser and Electro-Optics 1997 (CLEO/Pacific Rim '97) , in Chiba, Japan, 1997 July

[2.6] Y.Toda, K.Suzuki, and Y.Arakawa
"Magneto-optical Spectroscopy of Single InAs/GaAs Quantum dots"
The 24th International Conference on the Physics of Semiconductor (ICPS'98), Jerusalem, Iarael, 1998 August

[2.7] Y.Toda, S.Shinomori, K.Suzuki, and Y.Arakawa

"Near-field spectroscopy of a single InAs/GaAs quantum dot"
International Quantum Electronics Conference (IQEC '98), San francisco, USA, 1998 May

[2.8] K.Yamanaka, K.Suzuki, S.Ishida, and Y.Arakawa
"Light Emission from Individual Self-Assembled InAs/GaAs Quantum Dots Excited by Tunneling Current Injection"
International Solid State Device and Materials (SSDM'98)
Hiroshima, Japan, 1998 September

[2.9] K.Yamanaka, K.Suzuki, S.Ishida, T.Someya, and Y.Arakawa "Highly Spatially-resolved optical spectroscopy of single InAs quantum dot by STM"
Submitted to Optical Society of America (OSA'99) topical meeting, Colorado, U.S.A., 1999, April

[2.10] H. Hayashi, S.Ishida, K.Suzuki, K. Yamanaka, and Y. Arakawa
"Light Emission from Individual InGaAs/GaAs Self-Assembled Quantum Dots Excited by Tunneling Current Injection"
Nano-physics and Electronics ,B02, Tokyo, Japan, 1997 September

[2.11] K.Iizuka, K.Matsumaru, T.Suzuki, H.Hirose, K.Suzuki, and H.Okamoto
"Arsenic-free GaAs Substrate Preparation and Direct Growth of GaAs/AlGaAs MQW without Buffer Layer"
Eight International Conference on Molecular Beam Epitaxy (MBE-VIII), Osaka, Japan, 1994 August

(3) Domestic conference

[3.1] K.Suzuki and Y.Arakawa
"Self-assembled GaSb/GaAs Qunatum Dots Grown by Solid Source Molecular Beam Epitaxy"
17th Electronic Materials Symposium (EMS'98) Izu-Nagaoka, Japan, 1998 July.

[3.2] K.Suzuki, K.Tachibana, R.A.Hogg, and Y.Arakawa
"Growth and Optical Properties of Self-assembling GaSb/GaAs Quantum Dots by Molecular Beam Epitaxy"
Second Symposium on Atomic-scale Surface and Interface Dynamics, Gakushuuin University , Tokyo, Japan, 1998 February

[3.3] K.Suzuki and Y.Arakawa
"Optical properties of type-I InAs and type-II GaSb quantum dots" The 46th Spring Meeting, 1998; The Japan Society of Applied Physics and Related Societies, Tokyo Science University, March 1998.

[3.4] K. Suzuki and Y. Arakawa
"Smooth surface of GaSb buffer layer on GaAs using $(GaSb)_1(GaAs)_1$ superlattice"
The 59th Autumn Meeting, 1998; The Japan Society of Applied Physics, Hirashima University, September 1998.

[3.5] K. Suzuki, R. A. Hogg, K. Tachibana, and Y. Arakawa
"Formation of Type-II GaSb/GaAs Self-assembled Quantum Dots"
The 45th Spring Meeting, 1998; The Japan Society of Applied Physics and Related Societies, Tokyo Institute University, March 1998.

[3.6] K. Tachibana, K. Suzuki, and Y. Arakawa
"Fabrication of Self-assembled AlSb/GaAs V-grooves"
The 45th Spring Meeting, 1998; The Japan Society of Applied Physics and Related Societies, Tokyo Institute University, March 1998.

[3.7] K. Suzuki, R. A. Hogg, K. Tachibana, and Y. Arakawa
"MBE Growth of Quantum GaSb Dots on GaAs"
The 58th Autumn Meeting, 1997; The Japan Society of Applied Physics, Akita University, October 1997.

[3.8] R. A. Hogg, K. Suzuki, K. Tachibana, K. Hirakawa, and Y. Arakawa
"Optical Properties of GaSb Quantum Dots on GaAs"
The 58th Autumn Meeting, 1997; The Japan Society of Applied Physics, Akita University, October 1997.

[3.9] K. Suzuki, R. A. Hogg, L. Finger, and Y. Arakawa
"Optical Properties of AlGaAs-capped InAs Quantum Dots"
The 58th Autumn Meeting, 1997; The Japan Society of Applied Physics, Akita University, October 1997.

[3.10] K.Yamanaka, K.Suzuki, S.Ishida, T.Someya, and Y.Arakawa
"Highly Spatially Resolved (-20 nm) Optical Measurement of InAs Quantum Dots by STM" The 46th Spring Meeting, 1998; The Japan Society of Applied Physics and Related Societies, Tokyo Science University, March 1998.

[3.11] K. Yamanaka, K. Suzuki, S. Ishida, and Y. Arakawa
"Spatial Resolved Luminescence of Sigle Quantm Dots by STM "
The 59th Autumn Meeting, 1998; The Japan Society of Applied Physics, Hirashima University, September 1998.

[3.12] S. Shinomori, Y. Toda, K. Suzuki and Y. Arakawa
"Near-field spectroscopy of single quantum dots"
Second Symposium on Atomic-scale Surface and Interface Dynamics, Gakushuuin University , Tokyo, Japan, 1998 February

[3.13] S. Shinomori, Y. Toda, K. Suzuki, and Y. Arakawa
"Optical Near-field PL excitaion Spectroscopy of Single InAs Quantum Dots"
The 45th Spring Meeting, 1998; The Japan Society of Applied Physics and Related Societies, Tokyo Institute University, March 1998.

[3.14] Y. Toda, S. Shinomori, K. Suzuki, and Y. Arakawa
Near-field Spectroscopy of a Single InAs Iuntum Dot in High Magnetic Field"
The 45th Spring Meeting, 1998; The Japan Society of Applied Physics and Related Societies, Tokyo Institute University, March 1998.

[3.15] S. Kako, H. Watabe, K. Suzuki, Y. Naganune, K. Ujihara, H. Sakaki, and Y. Arakawa

"Magneto-Dependence of Carrier Drag Effect in Mesoscopic Structures"
The 45th Spring Meeting, 1998; The Japan Society of Applied Physics and Related Societies, Tokyo Institute University, March 1998.

[3.16] K. Yamanaka, K. Suzuki, S. Ishida, and Y. Arakawa
"Luminescence of Single Quantum Dots by STM"
The 45th Spring Meeting, 1998; The Japan Society of Applied Physics and Related Societies, Tokyo Institute University, March 1998.

[3.17] K. Yamanaka, H. Hayashi, K. Suzuki, S. Ishida, and Y. Arakawa
"Luminescence of Single Quantum Dots by STM"
The 58th Autumn Meeting, 1997; The Japan Society of Applied Physics, Akita University, October 1997.

[3.18] K. Suzuki, Y. Nagamune, Y. Ohno, T. Noda, H. Sakaki, and Y. Arakawa
"Temperature Dependence Negative Drift Mobility by Direct Obsevation of Carrier in Quantum Well"
The 57th Autumn Meeting, 1996; The Japan Society of Applied Physics, Kyushu Industry University, September 1996.

[3.19] K. Iizuka, K. Matsumaru, T. Suzuki, T. Konno, K. Suzuki, and H. Okamoto
"Arsenic-free GaAs Substrate Cleaning Method for MBE"
14th Electronic Materials Symposium (EMS'95) Izu-Nagaoka, Japan, 1995 July.

[3.20] K. Matsumaru, K. Iizuka, T. Suzuki, H. Hirose, K. Suzuki, and H. Okamoto
"High Temperature Surface Cleaning without As Flux of AlGaAs Grown by MBE (II)"
The 43rd Spring Meeting, 1995; The Japan Society of Applied Physics and Related Societies, Tohkai University, March 1995.

[3.21] T. Konno, K. Suzuki, T. Matsusue, H. Okamoto, K. Matsumaru, K. Iizuka, and T. Suzuki
"MBE Regrowth on AlGaAs by High Temperature Surface Cleanig without As flux"
The 43rd Spring Meeting, 1995; The Japan Society of Applied Physics and Related Societies, Tohkai University, March 1995.

[3.22] K. Matsumaru, K. Iizuka, T. Suzuki, H. Hirose, K. Suzuki, and H. Okamoto
"High Temperature Surface Cleaning without As Flux of AlGaAs Grown

by MBE"
The 55th Autumn Meeting, 1994; The Japan Society of Applied Physics, Meijoh University, September 1994.

[3.23] K. Suzuki, T. konno, T. Matsusue, and H. Okamoto
"Effects of absorption by excitions under electric fields in a sawtooth superlattice"
The 55th Autumn Meeting, 1994; The Japan Society of Applied Physics, Meijoh University, September 1994.

[3.24] K. Iizuka, T. Suzuki, H. Hirose, H. Okamoto, K. Suzuki, and S. Inoue
"High Temperature Surface Cleaning of GaAs Substrate without As flux for MBE growth"
The 42th Spring Meeting, 1994; The Japan Society of Applied Physics and Related Societies, Meiji University, March 1994.